Modelling Simul. Mater. Sci. Eng. **17** (2009) 084007 (35pp) doi:10.1088/0965-0393/17/8/084007

Simple intrinsic defects in gallium arsenide

Peter A Schultz[1] **and O Anatole von Lilienfeld**

Multiscale Dynamic Materials Modeling Department, Sandia National Laboratories, Albuquerque, NM 87185-1322, USA

E-mail: paschul@sandia.gov

Received 16 July 2009, in final form 8 October 2009
Published 23 November 2009
Online at stacks.iop.org/MSMSE/17/084007

Abstract

We investigate the structural properties and energy levels of simple intrinsic defects in gallium arsenide. The first-principles calculations (1) apply boundary conditions appropriate to charge defects in supercells and enable quantitatively accurate predictions of defect charge transitions with a supercell approximation, (2) are demonstrated to be converged with respect to cell size and (3) assess the sensitivity to model construction to Ga pseudopotential construction (3d core or 3d valence) and density functionals (local density or generalized gradient approximation). With these factors controlled, we present the first quantitatively reliable survey of defect levels in GaAs, reassess the available literature and begin to decipher the complexity of GaAs defect chemistry. The computed defect level spectrum spans the experimental GaAs band gap, defects exhibit multiple bistabilities with (sometimes overlapping) negative-U systems, express more extensive charge states than previously anticipated and collectively suggest that our atomistic understanding of GaAs defect physics needs to be reassessed.

(Some figures in this article are in colour only in the electronic version)

1. Introduction

Intrinsic defects play a prominent role in the fabrication and electronic performance of semiconductor devices. Self-diffusion governs the growth, transport and chemical evolution in a material. Defects react with dopants and impurities to introduce unwanted effects, scatter or capture free carriers, electrons and holes, affecting currents in electronic devices and gain in transistors. Immense effort has been directed toward identifying and quantifying the properties of defects in common semiconductors. In elemental silicon, a vast understanding of defect properties and their chemistry has been accumulated [1]. Other than silicon, gallium arsenide is perhaps the most studied semiconductor, arguably the most technologically important

[1] Author to whom any correspondence should be addressed.

compound semiconductor. Yet, despite intense attention, documented in a series of extensive reviews scattered over several decades [2–4], an atomistic understanding of defects in GaAs is not near as well developed as in silicon.

A quantitative, mechanistic description of defects and their chemistry is required for a thermodynamical analysis to address the technological questions important to device performance in GaAs [4]. Simple intrinsic defects are of paramount importance in radiation-damage devices, being the primary products of displacement damage. A few intrinsic defects exist in as-grown GaAs, the EL2 being the most important, but a more extensive variety of defects is generated by irradiation. Irradiation studies are a prime means to investigate intrinsic defects. Indeed, one early review declared that most of the intrinsic defects in GaAs had been identified in electron irradiation experiments [3]. That assertion has proven perhaps overly optimistic. Even the identity of the EL2, the signature defect that dominates the electronic properties of GaAs, remained contentious for many years, and its association with the arsenic antisite defect—an arsenic atom replacing a gallium in the lattice—is still occasionally disputed even in recent years. For other intrinsic defects, experimental identifications are even more tenuous.

The key to unlocking the detailed mysteries of defects in silicon was the use of electronic probes such as deep level transient spectroscopy (DLTS) to determine defect energy levels, coordinated with electron paramagnetic resonance (EPR) to determine defect structures. In the EPR, the superhyperfine interaction of an electron spin with neighboring nuclear spins gives a detailed mapping of the electronic defect state over atoms near the defect. The (dis)appearance of a defect level and the simultaneous (dis)appearance of an EPR spectrum identify the defect structure corresponding to the defect level. In GaAs this association of DLTS level measurement and EPS observed structure is broken [3, 5]. While silicon is ideal for EPR, consisting of 5% abundant spin-$\frac{1}{2}$ ^{29}Si, all As and Ga isotopes possess $\frac{3}{2}$ nuclear spins, with large, broad hyperfine spectra that swamp the superhyperfine splitting and prevent direct chemical identification of atoms involved in a defect. Without the fingerprint of EPR, defect identification and characterization in GaAs has been more challenging.

First-principles calculations using density functional theory (DFT) [6, 7] can compute detailed properties of point defects in semiconductors. In principle, DFT could stand in the place of EPR, to partner with DLTS to connect defect structures to observed defect processes in GaAs. Very early, Baraff and Schlüter used DFT to compute the properties of many simple point defects in GaAs [8], and Zhang and Northrup [9] extended these calculations with atomic chemical potentials and computed absolute formation energies of native defects in GaAs. These early studies used primitive computational models (small supercells, limited k-point sampling, small basis sets, etc) with limited accuracy, but set the precedent for DFT calculations being potentially useful for GaAs defect studies. These and subsequent simulations of GaAs defects were hampered, however, not only by computational limitations, but, more fundamentally, by a lack of a robust, rigorous method to compute defect energy levels, a problem compounded by the DFT 'band gap problem' [10]. The Kohn–Sham (KS) eigenvalue gap badly underestimates the experimental band gap. These problems inspired different compromises and approaches in different studies, leading to the embarrassing consequence (for simulation) that different calculations of defect level rarely agree with one another for calculations of defect levels. For example, in a list compiled by El-Mellouhi and Mousseau [11], ten independent theoretical calculations for the gallium vacancy in GaAs report nearly as many different sets of computed defect energy levels, bearing little resemblance to each other. It is small wonder that the insufficient accuracy of first-principles calculations was cited by Hurle [4] as a cause for dismissing first-principles simulations as a source of reliable values for use in thermodynamical analyses of defect effects in GaAs.

Modern computational resources and codes designed to take advantage of them have advanced over time, now enabling routine DFT calculations with hundreds of atoms, where 32- or 64-atom calculations were *tour-de-force* efforts only ten years ago. A more fundamental problem stemmed from the use of the supercell approximation [12, 13]: in practical calculations, an isolated defect is approximated using a periodic array of defects. Computing defect levels requires calculations of defects with a net charge, but a periodic charge in a supercell introduces infinities making it difficult to reconstruct a quantitatively meaningful energy expression. A variety of remedies based upon using a flat background charge to neutralize the net charge have been proposed [14–17]. An alternative approach is to use the full charge density in solving for the Coulomb potential, exploiting the linearity in the Poisson equation to solve the part of the potential due to the net charge with aperiodic boundary conditions and explicitly avoiding the periodic charge that leads to the unphysical infinities [18, 19]. Recently, we demonstrated that a total energy method for computing charged defects based on this approach, rigorously treating the boundary conditions and taking into explicit account finite size effects of the supercell approximation (such as bulk polarization), predicts accurate defect levels in silicon, within 0.1–0.2 eV of experimental values, for a wide array of defects [20]. Here, we apply this approach to simple intrinsic defects in GaAs, with comparable success.

In GaAs, the band gap problem is potentially more severe than in silicon [21], to the point where the band gap is so narrow that defect states cannot be identified. This is entangled with the technical question of what constitutes an adequate pseudopotential (PP) for Ga—whether the 3d electrons can be treated as core electrons or must be treated as valence electrons—and also with the question whether the local density approximation (LDA) or the generalized gradient approximation (GGA) performs better for GaAs. The fidelity of a functional fundamentally limits the accuracy of DFT calculations in predicting material properties [22]. Our earlier work [21] investigated the suitability of different PP and functionals for bulk properties of GaAs, and found that the PP construction could be manipulated to yield significant changes in the KS band gap, without compromising the predictions of bulk properties of GaAs. In this study, we examine whether a PP with the d-electron in the core is suitable for GaAs defect studies, and compare GGA and LDA for predictions of defect levels.

We present a broad computational survey of simple intrinsic defect in GaAs, computing charge states, structures and defect energy levels. Extensive experimental data have been collected over several decades, yet few unambiguous defect identifications have been made, outside the EL2, suggesting that all assumptions concerning defect identities need to be reinvestigated. We examine both monovacancies, v_{Ga} and v_{As}, and the divacancy, vv, both antisite defects, $\mathrm{As_{Ga}}$ and $\mathrm{Ga_{As}}$, and the di-antisite, which we label aa, and both self-interstitials, $\mathrm{Ga_i}$ and $\mathrm{As_i}$. We compute all the defect levels with a single consistent method, against a fixed electron reservoir, in a manner that determines the relative defect energy level positions without any arbitrariness. With the construction of the computational model carefully controlled and converged, we can make relatively confident predictions of defect levels, sufficiently reliable to begin to associate our defect results with observed experimental processes. As in the previous study on silicon defects [20], we find that the defect level spectrum in GaAs is not hampered by a band gap problem. The 'simple' intrinsic defects prove not to be so simple, supporting more charge states than previously believed, rife with bistabilities leading to several negative-U systems, even having as many as three negative-U systems within a single defect. Despite the unexpected complexity, a few simple chemical motifs emerge that explain much of the ground state bonding. Taken collectively, these new results challenge some long-held beliefs about radiation-induced defects, and invite a reassessment of defect behavior in GaAs.

Table 1. Theoretical bulk properties computed with the PPs used in this study, and a comparison with available experiment.

	Simulation context			
	LDA-3d	LDA	PBE	Expt.
GaAs				
a_0 (Å)	5.628	5.599	5.739	5.65 [26]
B (GPa)	77.0	72.4	59.6	79 [26]
E_g (eV)	0.47	0.83	0.45	1.52 [27]
ΔH (eV)	0.636	0.740	0.787	0.74 [28]

2. Computational methods

2.1. Computational setup

All density functional calculations were performed with SEQQUEST [23], a periodic PP code using well-converged contracted-Gaussian basis sets. This code is highly accurate, computationally efficient for large systems, and the local basis set is particularly advantageous for calculations involving the 3d electrons of the gallium atom as valence electrons. We used the Perdew–Zunger formulation of the LDA [24] and the Perdew–Burke–Ernzerhof (PBE) [25] form of the GGA.

Previously, we had explored the effect of PPs on the prediction of structure and band gap in GaAs [21], prompted by the observation that the 'best' PP constructions—the one best approximating the all-electron limit—yielded a DFT eigenvalue gap so small as to be unusable for defect calculations. It would not be possible to locate defect states in the gap. Different PP constructions and functionals produce larger DFT eigenvalue gaps, while still retaining the accuracy of DFT for bulk structure ground state properties. The two most important factors were, first, whether the $3d^{10}$ electrons of the gallium were left in the valence or placed in the core and, second, the functional, LDA or PBE. The attraction of a 3d-core PP is the much reduced computational cost of eliminating the 3d electrons from the valence DFT calculation, but this entails the potential compromise of fidelity, as designing a robust, transferable 3d-valence PP for Ga is a challenge. We use three sets of PP in the defect calculations to assess the importance of PP and functionals: (1) LDA, with 3d electrons in the core, (2) LDA-3d, with a 3d-valence PP and (3) PBE, with a 3d-core PP. The standard LDA and PBE PP correspond to the 's^+H' PP (3d core) and the 'LDA-3d' set corresponds to the 's^+Hd' PP (3d valence) defined in the previous study [21], to which we refer the reader for further details. We use the extended As($l = 3$) PP in the GaAs calculations [21].

As in the bulk study, valence double-zeta plus polarization basis sets are used on all atoms. In vacancy defect calculations, the atom-centered basis is augmented with 'ghost atoms': a set of single-Gaussian s, p and d floating orbitals with decay constants of 0.12, 0.14 and 0.16 (atomic units) is placed at each vacant site (both As and Ga). In test calculations for both the arsenic vacancy and gallium vacancy, there was less than 20 meV total energy lowering per site upon adding these floating orbitals, attesting to the adequacy of the atomic basis sets even without augmentation.

Table 1 summarizes theoretical bulk properties obtained with the PPs used in this work. The calculations for the elemental solids were also carefully converged, and yielded very good agreement with the experiment for elemental Ga in the $A11$ structure [29] and elemental As in the $A7$ structure [30]. The resulting computed heats of formation ΔH for GaAs are also in good agreement with the experimental value of 0.74 eV [28].

The defect calculations use cubic supercells with 64, 216 and 512 atoms in the crystal supercell. The lattice parameter is fixed to the theoretical value (see table 1). The Brillouin zone is sampled with regular k-space grids, 3^2 in the 64-site cell and 2^2 in the 216- and 512-site cells, offset from the Γ point, converged for each of these cell sizes. The defect configuration is relaxed until forces on every atom are less than 0.0004 Ry bohr^{-1} ($\sim$0.01 eV Å^{-1}), converging the total energy to better than 1 meV. As the accuracy of DFT itself is no better than 0.1 eV, and we quote defect level results only to 0.01 eV, this tolerance is sufficient. We use real space integration grids equivalent to a 36^3 grid in an 8-atom supercell for LDA and PBE (e.g., a 108^3 grid in the 216-site cell), and a 48^3 grid for the more computationally challenging LDA-3d simulations. These grids were determined to give converged energies and structures, verified in every defect supercell relaxation to give consistent energy lowering as the atomic configuration was relaxed along the direction of the atomic forces. We use an efficient accelerated steepest descent method in defect systems with a complicated potential energy surface to ensure the system would relax to a minimum rather than to some other critical point. We use a modified Broyden method due to Johnson [31] to optimize a minimum in a well-defined potential basin, and also to refine saddle point configurations for migration barrier calculations. Candidate geometries for a barrier calculation are obtained using a nudged elastic band (NEB) method [32] to construct a chain of configurations along a minimum energy path connecting two different defect configurations, and selecting the atomic configuration closest to the high-energy barrier.

2.2. *Finite defect supercell model*

We use the theoretical machinery of the finite defect supercell model (FDSM) [20] to provide a controlled approximation for computing the energies of charged supercells. The local moment counter charge (LMCC) method is used to remove the artificial periodic images of the net charge in the cell and self-consistently evaluate the correct local potential due to a localized, aperiodic charge [18]. To compute meaningful charge transition energies, a fixed chemical potential for charge is established through contact with a perfect crystal potential [19], functionally equivalent to setting the defect potential and crystal potential equal infinitely far from the defect. A discrete defect occupation scheme [20] is used to mitigate defect dispersion effects, and ensures a consistent defect state is populated across all k points. And, finally, a simple dielectric approximation [33] is used to evaluate the bulk polarization energy outside the volume of the DFT supercell (rydberg atomic units) [20]. The bulk polarization energy $E_{\rm pol}$ of a structureless dielectric outside a spherical cavity of radius $R_{\rm Jost}$ containing a point charge (rydberg atomic units) is

$$E_{\rm pol}(q) = (1 - 1/\epsilon_0)(q^2/R_{\rm Jost}). \tag{1}$$

The charge q is the charge on the defect. For the static dielectric constant, we use the experimental value $\epsilon_0 = 13$ [26]. The polarization energy is only weakly dependent on ϵ_0, justifying very cursory attention to the exact value of this parameter. The polarization is much more sensitive to the choice of $R_{\rm Jost}$. Naively, $R_{\rm Jost}$ would simply be set to the radius of a sphere of the same volume as the supercell. However, as Lento *et al* noted [34], electrons are drawn from the exterior of the supercell to screen the interior region near the defect charge, leaving the outer part of the supercell unscreened. An effective $R_{\rm Jost}$ should be smaller than the radius defined by the total supercell volume. In silicon this was not a significant effect, the largest charge on a defect was ± 2, and an unscreened skin depth of 0.8 bohr (an $R_{\rm Jost}$ smaller by 0.8 bohr than the radius matching the supercell volume) proved good enough, yielding 0.1 eV accuracy in the defect level calculations [20]. In GaAs, having defect up to $|q| = 4$

Table 2. Supercell size dependence of selected formation energies and charge transitions, in eV, after bulk polarization term is included. The v_{Ga} charge transitions were used to calibrate the bulk polarization, and are referenced to the $v_{Ga}(0/1-)$. The $As_{Ga}(0)$ formation energy and the splitting between its levels is presented as a check of the adequacy of this calibration. Note the energies are quoted to 0.001 eV, to distinguish the small differences between results for different cell sizes.

	Supercell size		
	64 site	216 site	512 site
v_{Ga}—unrelaxed			
$v_{Ga}(0)$	3.167	3.244	3.327
(1−/0)	0	0	0
(2−/1−)	0.314	0.281	0.275
(3−/2−)	0.654	0.621	0.615
v_{Ga}—relaxed			
$v_{Ga}(0)$	2.814	2.691	2.745
(1−/0)	0	0	0
(2−/1−)	0.174	0.153	0.141
(3−/2−)	0.341	0.321	0.303
As_{Ga}—relaxed			
$As_{Ga}(0)$	1.534	1.500	1.507
(0/1+)	0	0	0
(+/2+)	−0.230	−0.248	−0.251

and with a q^2 dependence in the bulk polarization term, this term needs to be more carefully calibrated.

We use the negative charge states of the Ga vacancy to calibrate R_{Jost}, and determine that a skin depth of 1.6 bohr is best for the GaAs defect supercell calculations. The simple Ga vacancy, as described later, retains a tetrahedral configuration that does not change much going from the neutral to the (3−) charge state. In table 2 we present the supercell dependence of the formation energy of $v_{Ga}(0)$ and the relative charge transition energies, referenced to the (−1/0) transition energy. The steps between charge transitions in the 216-site cells and 512-site cells almost exactly match for the unrelaxed v_{Ga}—the (2−/1−) transition being 0.28 eV above the (1−/0) transition and the (3−/2−) being 0.62 eV above (1−/0)—and the 64-site cells transitions differ from these by only 0.03 eV. Using the relaxed configuration for v_{Ga}, the steps are also well converged, indicating the cell-size dependence of the bulk polarization has been accounted for correctly. Interestingly, the charge transitions converge better than the formation energy of the neutral vacancy. The formation energy includes the full interactions between defect images, but each charge transition involves only a single electron, a useful cancellation of errors. This skin depth was calibrated using only the v_{Ga}, and then the same skin depth R_{Jost} was used for every charged defect calculation. The effectiveness is checked in the results presented for As_{Ga} in table 2, where the splitting in the As_{Ga} donor levels shows no cell-size dependence after applying the bulk polarization correction using an unscreened skin depth of 1.6 bohr.

2.3. Defect formation energies and defect level computation

Unless otherwise noted, all defect formation energies are quoted in the As-rich limit, using converged, fully cell-relaxed calculations of the *A*7 structure as the As reference. The FDSM formation energy E_{form} [20] of a charged defect in GaAs with n_{Ga} Ga atoms and n_{As} atoms in

the defect supercell can be expressed as

$$E_{\text{form}}(q) = E_{\text{def}}(q) + E_{\text{def}}^{\mu_e}(q) + E_{\text{pol}}(q) - n_{\text{Ga}}\mu_{\text{Ga}} - n_{\text{As}}\mu_{\text{As}}, \tag{2}$$

where $E_{\text{def}}(q)$ is the energy reported by the DFT supercell calculation, $E_{\text{def}}^{\mu_e}(q)$ connects the energy of the net charge q in the cell to a electron reservoir defined by a perfect crystal supercell calculation and $E_{\text{pol}}(q)$ is the bulk polarization energy outside the supercell. This last term is an analytic extrapolation from the finite supercell to the result in an infinite supercell. In the As-rich limit, the arsenic chemical potential $\mu_{\text{As}} = \mu_{\text{As}}^{A7}$, and the gallium chemical potential μ_{Ga} is determined as

$$\mu_{\text{Ga}} = \mu_{\text{GaAs}}^{\text{bulk}} - \mu_{\text{As}}^{A7}, \tag{3}$$

where $\mu_{\text{GaAs}}^{\text{bulk}}$ is the energy per GaAs formula unit in the perfect crystal supercell from which the defect calculation is constructed, thus defining the chemical potentials to give a zero formation energy of bulk GaAs. The thermodynamically permissible chemical potentials for the As atom range from arsenic-rich, $\mu_{\text{As}} = \mu_{\text{As}}^{A7}$, to gallium-rich, $\mu_{\text{As}} = \mu_{\text{GaAs}}^{\text{bulk}} - \mu_{\text{Ga}}^{A11}$. Knowing the heat of formation, as listed in table 1 and the stoichiometry of the defect, it is straightforward to convert values from one limit to the other [9].

The total energy of every charged defect supercell is referenced to an electron reservoir in the perfect crystal. The electron chemical potential is thus the same for every defect calculation in a supercell, but the position of this reservoir relative to vacuum or a band edge is unknown. The defect levels are computed as ionization potentials referenced to this common reservoir, differences in computed ground state total energies of the defect in different charge states, total energies that do *not* at any point incorporate a KS eigenvalue or differences in KS eigenvalues in their evaluation.

The KS eigenvalues are formally not predictors of total energies [35] and are quantitatively inaccurate for use in calibrating the relative total energies of defects, or the position of a defect energy level with respect to a band edge. The KS eigenvalues do not represent good approximations to the energies of the band edges, moreover, the difference between the band edge KS eigenvalues, the KS band gap, is not a valid approximation to the total energy KS gap. As we shall see below, the defect band gap obtained by the results of strictly total energy calculations is disconnected from the KS eigenvalue gap. The ionization potential corresponding to the valence or conduction band edge cannot be computed in a method compatible with the defect ground state total energies.

We use the full spectrum of computed defect ionization potentials, with the relative defect level positions fixed by the use of a common, but unknown, chemical potential, and infer the location of the band edges in that spectrum. In silicon, with extensive experimentally identified levels, the position of the valence band (VB) and conduction band (CB) in relation to the spectrum of computed defect ionization potentials could be set where the experimental and theoretical defect energy level spectra best coincided. In GaAs, few defect levels are experimentally identified and this calibration is not as definitive. However, with a large number of computed defect levels, we take the VB and CB positions to be just outside the spectrum of defect states, i.e. the smallest and largest ionization potentials that are clearly identified as defect states. The simple intrinsic defects have, collectively, a large number of levels in the lower half of the gap, we set the VB position at the ionization potential corresponding to where certain defect hole states began to be contaminated with the VB and before other states were fully immersed in the VB. The upper half of the band had either clean defect states, or a defect calculation was fully immersed in the CB; we arbitrarily set the CB edge just above the highest defect level.

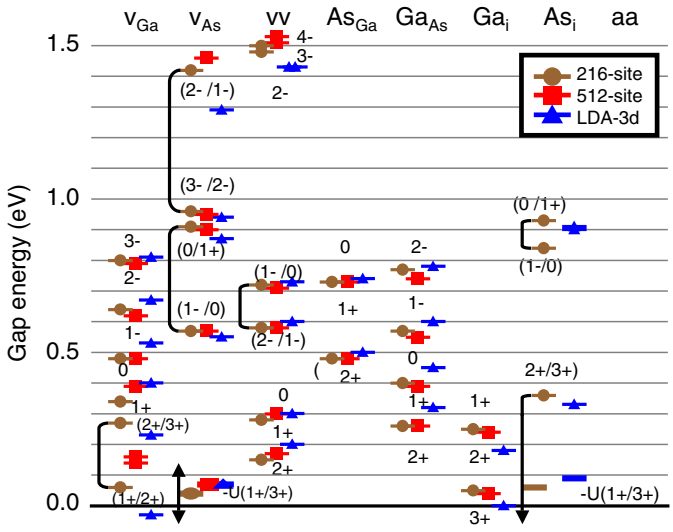

Figure 1. Computed LDA defect energy levels for simple intrinsic defects in GaAs. The Ga 3d-core PP results extrapolated to infinity using 216-/512-site supercell results are marked with (brown/red) circles/squares. The 3d-valence results for 216-site cells marked with (blue) triangles. Levels connected with vertical lines are negative-U systems (not just the 216-site results as explicitly connected, but also the associated 512-site and LDA-3d results). Note that we did not perform 512-site supercell calculations for As_i. (Color online.)

3. Defect results

The full defect level spectrum over all the intrinsic defects is presented in figure 1. The levels are computed as the thermodynamic values, difference in energies between the lowest energy structures of each charge state, without regard for whether a barrier in a bistability might prevent the transition from being observed in an electronic measurement due to kinetic limitations. The immediate notable observation is, just as in the case of silicon defects [20], the range of defect energy levels almost exactly matches the experimental band gap in GaAs, 1.52 eV [27]. From the position of the VB to an assumed CB edge just above the highest defect level, the $vv(4-/3-)$, the LDA defect band gap for GaAs is 1.54 eV. The KS gap with the LDA 3d-core PP is 0.83 eV. The LDA-3d KS gap is much smaller, only 0.47 eV, yet its defect band gap is also in good agreement with the experimental band gap. The band gap problem, stated as a KS gap that is too small, does not hamper quantitative calculations of defect levels over the entire experimental gap. That the defect band gap is not sensitive to the KS gap is auspicious for defect studies in GaAs, apparently the PP can be manipulated to modify the KS gap without affecting the defect energetics. Deep level defects do not follow the band edges, they are entirely decoupled from the band states, and one does not need to apply any scissors operator or other ad hoc procedure to get accurate defect levels, existing LDA and PBE functionals already give good results.

The infinite-limit defect energy levels computed using the 512-site supercell results almost exactly align with all the levels obtained using the 216-site supercell results, to within 0.03 eV. This agreement simultaneously demonstrates that the defect calculations are converged with respect to cell size, and that a 216-site supercell is sufficient for defect level calculations for GaAs, and with respect to k-point sampling (the two cells have different densities of k points). The sole exception is for the individual charge transitions comprising the $v_{Ga}(1+/3+)$

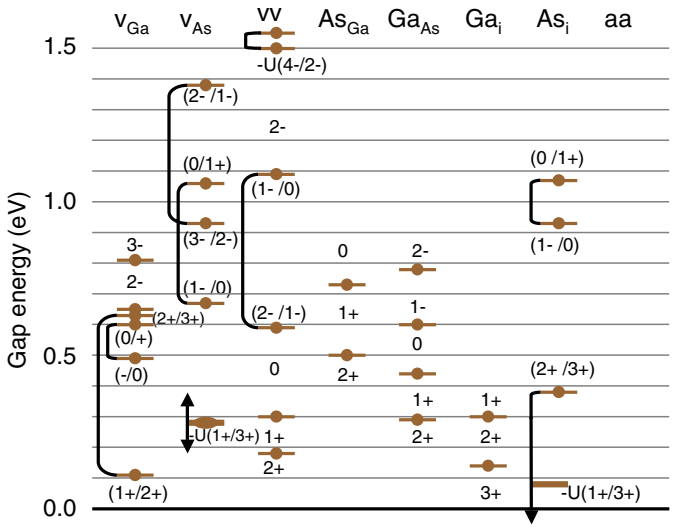

Figure 2. Computed PBE defect energy levels for simple intrinsic defects in GaAs, extrapolated to infinite supercells from results of 216-site supercell calculations. Levels connected with vertical lines are negative-U systems. (Color online.)

negative-U level. The $v_{Ga}(2+)$ state is partially contaminated with the VB, its energy and the charge transition energies involving it are compromised. The full negative-U $v_{Ga}(1+/3+)$ levels do align between the two supercells. The near-perfect alignment between all the defect levels, not only for idealized symmetric defects, but defect transitions involving large lattice relaxation, reduced-symmetry, negative-U systems, proves the effectiveness of the FDSM model to properly treat the boundary conditions of charged defect supercells, and lends confidence to the DFT predictions. With this demonstrated alignment, the bulk polarization model passes a particularly stringent test very well. Many defects possess charges with ± 3 or even one $(4-)$, and the q^2 dependence in the bulk polarization would magnify any errors in the model, yet the highly charged defect levels show no greater errors than the minimally charge defects.

The gallium PP does not have a big effect on the defect energy levels. All the qualitative features of the LDA defects are mimicked by the LDA-3d. Most of the LDA and LDA-3d levels are within 0.05 eV of each other, except for the highest acceptor states of v_{As} and vv, which differ by 0.1–0.2 eV. The general agreement suggests that the 3d-valence PP may be unnecessary for intrinsic defects in GaAs. The differences between the 3d-core and 3d-valence results are smaller than the errors expected from the use of the DFT approximation. This could be quite useful for modeling; the 3d-core PPs are computationally cheaper (especially for plane wave codes), and yield larger KS band gaps that are better suited for defect studies.

The defect levels computed with PBE are presented in figure 2. Once again, the defect band gap agrees well with the experimental band gap, despite a KS band gap of only 0.45 eV, much smaller than the LDA gap. All the defects have the same range of charge states, and the transitions are qualitatively the same as the LDA. The quantitative differences are more significant, in particular, the negative-U systems, caused by rebonding and large lattice relaxations, tend to be stronger. Unlike the Ga PP, which proves to be of marginal importance, the functional might play a more important role in quantitative defect calculations in GaAs.

The simple instrinsic defects of GaAs, and particularly the vacancies, are notable for having many charge states, with the divacancy sustaining a full $(4-)$ charge. Many exhibit

(multiple) bistabilities, with numerous negative-U systems. The unexpected complexity of the intrinsic defects partially explains why it has proven so difficult to characterize GaAs defects in experiment. In the following, we describe the defects in their full complexity. The EL2 center is the best characterized defect in GaAs, with a number of fascinating, distinctive and well-defined properties [36]. The EL2 is a double donor, with the first donor level near midgap, $E_c - 0.75$ eV, and a second donor level ∼0.3 eV below that [37], at $E_v + 0.54$ eV [38, 39]. At low temperatures, the neutral EL2 can be optically bleached, transform into a metastable EL2* state, rendering the defect electrically invisible. The electrically active EL2 is reversibly regenerated from the EL2* when the temperature is increased above 140 K, over an energy barrier of ∼0.3 eV. The EL2 has been unambiguously demonstrated to contain an arsenic antisite, and the evidence is compelling that the EL2 is simply an isolated As_{Ga} rather being complexed with other defects [40–43]. As the only clear assignment for any simple intrinsic defect in GaAs, we begin with the arsenic antisite and its relationship to the EL2 center in GaAs, to validate the calculational approach in this study for the description of defects in GaAs. We begin with a detailed comparison of our results to the existing experimental lore for the EL2, and then proceed to present results for the other intrinsic defects.

3.1. The arsenic antisite, As_{Ga}*, and the EL2 center*

Early theory demonstrated that an isolated neutral arsenic antisite As_{Ga} exhibits a metastability consistent with the EL2 [36, 44]. The fundamental T_d substitutional configuration could be optically excited into a C_{3v} metastable configuration: the central substitutional As breaks one bond with a neighboring arsenic atom, puckering through the plane of the other three arsenic neighbors toward a nearby interstitial site, as illustrated in figure 3. In the undistorted antisite, figure 3(*b*), the As has two electrons more than can be accommodated in the bonds to its neighbors, making it a double donor. In the distorted As^*_{Ga}, figure 3(*b*), one As–As bond around the central atom is broken, and the other three bonds are strained far from their preferred tetrahedral orientation.

Our results match this description of As_{Ga} [36, 44]. The T_d antisite has three stable charge states, ranging from neutral to (2+). The neutral antisite has a T_d symmetric ground state, and a metastable C_{3v} configuration where the central As atom distorts in a [1 1 1] direction away from the antisite, the As^*_{Ga}. The donor levels of the symmetric As_{Ga} sink below the VB edge, thus the positive charge states disappear in the distorted As^*_{Ga}.

The qualitative picture for the bonding and metastability has a simple chemical explanation. The energy cost for breaking the As–As bond and the strain in the bonding around the distorted As atom is almost fully compensated by the energy stabilization from the capture of the two donor electrons into valence states, into the lone pairs created on the newly three-fold-coordinated arsenic atoms, as depicted in figure 3(*c*). These As lone pairs are underneath the VB edge and electrically inactive, and the As^*_{Ga} has no donor levels. Such a large stabilization and lack of donor levels suggest a significant electron affinity of the arsenic lone pairs, an observation that becomes important later in explaining the structure and metastability in vacancy defects in GaAs.

The structural landscape for the neutral antisite is depicted in figures 3(*d*) and (*e*). Using the LDA, the formation energy of the T_d ground state neutral antisite is 1.50 eV, and the metastable is 0.43 eV higher. This As_{Ga} formation energy is consistent with previous LDA calculations [9, 45, 46], although, mysteriously, the LDA supercell calculations most similar to the current study (216 site, 2^2k sampling), due to Schick *et al* [47] differ most, reporting a larger formation energy of 1.8 eV. The saddle point barrier was obtained in two steps, as described in the Methods section. First, we used a NEB calculation to identify intermediate

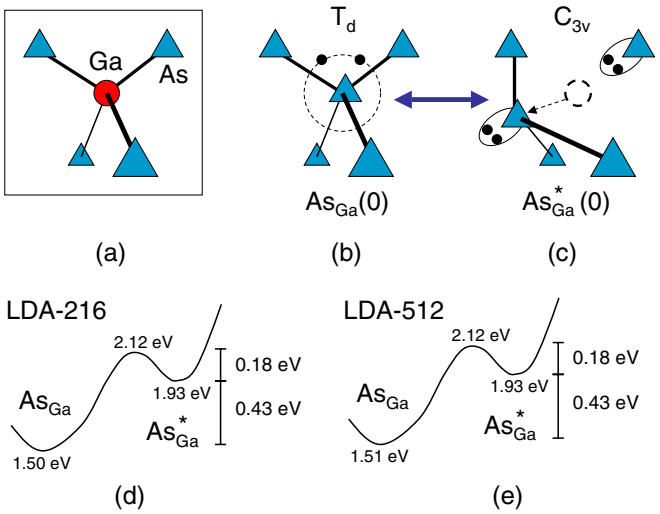

Figure 3. Schematic depiction of the bonding in the arsenic antisite, As_{Ga} and its metastable configuration, As^*_{Ga}, and the energetics of the transition between them. A Ga atom in the perfect crystal (*a*) is substituted by an arsenic atom to form (*b*) the ground state $As_{Ga}(0)$. The two extra valence electrons of the As atom (with respect to the Ga atom it replaces), orbit the center in a localized Rydberg (non-bonding) state. In the metastable state, the substitutional As retreats along a [1 1 1] direction toward an open interstititial site, breaking one As–As bond, and straining the others. The two extra electrons are captured in the dangling bonds, forming complete lone pairs, the electron affinity of the lone pairs compensating for the energy cost of breaking the bond and introducing local strain. In (*d*) and (*e*), the energetics of the transitions are schematically depicted for the 216-site and 512-site LDA calculations, respectively. The formation energies of the antisite for the two cells are nearly identical (within rounding errors), and the $As^*_{Ga}(0)$ is higher than the ground state $As_{Ga}(0)$ by 0.43 eV, with a barrier of 0.18 eV separating it from the ground state potential well. (Color online.)

configurations along a minimum energy path between the ground state and distorted state configurations. Then, starting from a configuration nearest the barrier, we refined the saddle point geometry to atomic forces less than 3 meV $Å^{-1}$ using a modified Broyden method due to Johnson [31]. The computed barrier to return from the distorted C_{3v} to the T_d is 0.18 eV. These values are in (fortuitously) good agreement with the 0.38 eV difference and 0.20 eV barrier originally reported [44] using only an 18-site supercell. The computed barrier agrees well with the experimentally observed barrier of 0.3 eV [48–50].

The structural energetics are consistent across the different simulation contexts. The LDA-3d simulation values, a 1.48 eV formation energy, 0.42 eV difference, and 0.19 eV barrier, mimic the LDA results. This mimicry is not surprising given that the immediate environment of the distorted antisite has only arsenic atoms, and also implies that the perturbed region around the antisite is mostly localized within those immediate neighbors. The PBE simulation 1.27 eV formation energy is somewhat smaller, but the energy landscape otherwise very closely follows the LDA landscape: the PBE distorted state is 0.52 eV higher than the T_d ground state, with a 0.20 eV barrier to return.

The LDA 512-site supercell calculations almost exactly match (within 0.01 eV) the results for the 216-site calculations. The 64-site calculations (1.53 eV formation, 0.39 eV difference, 0.20 eV barrier) are also very close to the 216-site calculations. This indicates that, despite the significant strain present in the distorted As^*_{Ga}, this strain is fully resolved within a very short distance from the defect. Furthermore, the extent of the donor electrons in the T_d geometry must be short ranged, already mostly contained within the volume defined by the 64-site

supercell, otherwise the defect–defect interactions between supercells would lead to different computed formation energies for the neutral defect in the different supercells.

The strong localization suggests the As_{Ga} donor states will be deep levels. As seen in figures 1 and 2 the $As_{Ga}(0/+)$ level is midgap in every simulation context, LDA, PBE and LDA-3d. The $As_{Ga}(+/2+)$ level is 0.24 ± 0.01 eV below the $As_{Ga}(0/+)$ level in every simulation context, using different functionals, PPs and cell sizes. The consistency of the numerical description across different functionals and PPs suggests that the DFT is accurately describing this defect [22]. The close agreement across cell sizes demonstrates that the defect is well contained within a small volume and that results extrapolated from the supercell calculations are converged with rather small supercell sizes.

The EL2 defect seen in arsenic-rich native GaAs is observed to be double donor [37–39, 51]. Our computed midgap $As_{Ga}(0/+)$ donor state, at 0.80–0.81 eV below the CB, is consistent with experimental observations for the EL2(0/+) level, ranging from 0.74 to 0.83 eV below the CB edge [37–39, 51–58]. We reiterate that the DFT supercell calculations can only unambiguously calculate the positions of the defect levels with respect to one another, the position of a CB (or VB) edge with respect to a defect level cannot be directly computed. The good agreement between the computed level positions and experiment (assuming that the As_{Ga} is indeed correctly assigned to the EL2) is evidence that our inferred size of the DFT defect band gap (1.54 eV) and the positions of the band edge used in constructing the defect level spectrum in figures 1 and 2 are accurate. The apparent uncertainty in the positions the DFT defect band edges, $\sim$0.05 eV, is comparable to the variability in the experimental measurements of the EL2(0/+) defect level with respect to the band edge.

The 0.24 eV splitting between the computed As_{Ga} donor levels is in extraordinarily good agreement with the splitting between the EL2 levels observed in both p-type [38], (0/+) at $E_c - 0.75$ eV and (+/2+) at $E_v + 0.54$ eV and n-type [39] GaAs, with (+/2+) also reported at $E_v + 0.54$ eV. The computed splitting is insensitive to the position of the DFT defect band edge, and therefore this comparison has less uncertainty and is a more meaningful measure of the accuracy of the DFT predictions than the level positions themselves. This quoted agreement, within 0.01 eV, is better than could generally be expected using DFT. We note, however, that the calculations of the defect levels shown in figures 1 and 2 have not included spin, which could potentially impact the quality of the predictions.

The $As_{Ga}(1+)$ defect is lowered by 27 meV in LDA and 40 meV in PBE by adding spin polarization. This small lowering with spin is consistent with that seen in test calculations with other GaAs defects, and also matches earlier results of adding spin in Si defects [20]. Including spin polarization, the splitting between the As_{Ga} donor levels increases by 0.05 eV for LDA and 0.08 eV for PBE, raising the (0/+) level by the $As_{Ga}(1+)$ spin-polarization energy, and lowering the (+/2+) level by this spin-polarization energy. Including spin, the computed difference between the levels still agrees with experiment to within 0.1 eV, not as good as the 0.01 eV agreement seen without spin, but consistent with the general accuracy observed and expected from DFT calculations for semiconductor defects [20]. The minor numerical importance of spin justifies the neglect of spin effects in the broader set of GaAs defect calculations, motivated by the desire to reduce computational expense.

The earliest DFT calculations of Baraff and Schlüter [8] placed the As_{Ga} donor levels high in the gap (but with a separation, 0.25 eV, that closely matched the experiments). Zhang and Northrup [9] reported their calculated levels were midgap, but would be negative-U (by 0.05 eV). Chadi later stated the (0/+) to be approximately midgap, but only 0.04 eV higher than the (+/2+) level [59]. Other recent DFT results place the donor levels in the lower half of the gap, with either 0.1 eV separation [47] or 0.34 eV separation [60] between the donor levels. This variability can be ascribed to computational limitations (smaller cell sizes and k-point

sampling), and ambiguity in how to specify boundary conditions for charged supercells and defect levels calculations.

Our numerical results for the As_{Ga} metastability are converged with respect to cell size, and are insensitive to the choice of functional and the design of the PPs. These results match the properties of the EL2 very well: metastability, electrical activity, barrier to return. In addition, we have shown that the electrical levels of the As_{Ga} also match up very well with the observed levels of the EL2, using a method that can meaningfully compute relative defect energy levels. This internal consistency within the theory and the very good agreement with experiment for the size of the band gap and the properties of the EL2 serve as good evidence of validation of the computational approach used in this study. The EL2 is nearly the only definitively characterized defect in GaAs, and therefore is the only means by which to validate that the theory is accurately predicting GaAs defects correctly, and these simulations satisfy this requirement.

In total, the DFT results provide compelling evidence that the isolated As_{Ga} is indeed an EL2 center, and almost certainly the dominant EL2 center, yet significant mysteries remain surrounding the behavior of EL2. While the evidence is compelling that the EL2 is an isolated As_{Ga} defect [40–43], experimental observations exhibit greater complexity than can be explained by a simple antisite. For example, Fukuyama *et al* [50] presented experimental evidence that the EL2* has multiple paths for reorienting back to the fundamental EL2, with different barriers. An intriguing proposal to explain the complexity of behavior in the EL2 was offered by Chadi [59], who speculated that the isolated As_{Ga} could have, not one, but two distinct metastable structures. The second metastable structure descends from the first distorted EL2* by breaking a second As–As bond in the distorted As atom, and that this second distortion stabilized additional, negative charge states [59]. The observed complexity in EL2 was attributed to the intrinsic complexity of the As_{Ga}. This model had the significant virtue being consistent with the clear identification of the $EL2$ with an isolated antisite, and provided a rationale for more complex behavior. However, this model also has the unfortunate vice of proposing additional charge states for the EL2* defect that have not been observed. We searched for the Chadi structure, and were unable to locate a local minimum for this doubly distorted structure in either a neutral or a single negative charge state. This second distortion appears to be a computational curiosity that seems unlikely to be realized in GaAs.

3.2. The gallium antisite, Ga_{As}

The central gallium in the gallium antisite has two fewer valence electrons than the arsenic it replaces, and the Ga_{As} therefore is expected to be a double acceptor. The calculations in all simulation contexts exhibit two acceptor levels. There is a near coincidence of the Ga_{As} acceptor levels with the As_{Ga} donor levels. The $Ga_{As}(2-/1-)$ level, at $E_c-0.77$ or 0.78 eV (0.74 eV for the 512-site cell), is within 0.05 eV of the As_{Ga} in each simulation context, and the Ga_{As} $(1-/0)$ level is within 0.1 eV (higher) than the computed $As_{Ga}(1+/2+)$ state. The Ga_{As} levels could perhaps be mistaken for the As_{Ga} levels, if the Ga_{As} were present, except that the Ga antisite is an acceptor and that As antisite is a donor.

A double acceptor with levels at E_v + 77–78 meV and ∼0.2 eV has been observed, and tentatively attributed to the bare Ga_{As} $(-/0)$ and $(2-/-)$ charge transitions, respectively [3, 61, 62]. Our calculations are unambiguous in identifying the Ga_{As} acceptor states as near midgap. We expect the errors in the computed deep DFT levels to be no greater than 0.1–0.2 eV error seen in Si and in the As_{Ga} acceptor states (the EL2). To assign near-VB levels to the acceptor states of Ga_{As} would require an error of 0.5 eV in the computed energy level, twice as large as the largest error seen using the FDSM method in numerous defect level calculations

in either Si or GaAs. In the absence of a specific chemical identification of the defect in experiment, we conclude that these relatively shallow levels cannot be due to Ga_{As}, and must be attributed to a different defect, perhaps a donor complex [63].

Zhang and Chadi [64] proposed that the Ga antisite defect would be bistable, with a transition from a four-fold central Ga atom to a three-fold atom, and their resultant LDA energy levels formed a negative-U system near the VB. In tight-binding calculations, Seong and Lewis [65] echoed this prediction and, in addition, proposed that the Ga_{As} would have two *donor* charge states. The Ga_{As} defect levels in figures 1 and 2 were generated using the T_d-symmetric configurations.

The missing electrons in the Ga_{As} are from p-like states, being at the top of the VB, and therefore Ga_{As} has a degeneracy subject to a Jahn–Teller distortion [66]. An orbital degeneracy will couple to a lattice distortion, lowering the symmetry to lower the energy. However, in practical calculations within the supercell approximation, a distortion can be suppressed. The lattice constrains the distortion, and interaction between defects in different supercells leads to defect banding and tends to mix the different distorted electronic states. We explored a variety of local distortions of the neutral defect in different symmetries in LDA (216-site) calculations. We investigated C_{3v} as well as D_{2d}, resonant-D_{2d} and C_{2v} distortions, and find Jahn–Teller lowering from the T_d-symmetric state for all these distortions. However, none of the distortions are structurally significant, and the largest lowering of any distortion is less than 0.05 eV. Large distortions [64, 65] are not found.

Nonetheless, we discover Ga_{As} might take both 1+ and 2+ charge states, even in the absence of a large distortion. Because of the ambiguity in DFT defect calculations in distinguishing near-shallow states from band states, the positive charge states need to be very carefully and skeptically examined[2]. In any defect supercell, the DFT eigenstates are perturbed from a perfect crystal supercell, making it challenging to distinguish a defect state from a band state. For the Ga_{As} supercell, the Ga antisite-derived states are embedded in the bonds with the GaAs network, making this distinction particularly challenging. The replacement of the As with Ga leads to less strongly held electrons in the Ga–Ga bonds. The KS gap in the Ga_{As} cell is less than the crystal KS gap, these Ga–Ga bond states apparently lifting the VB edge in the defect supercell, offering the possibility that Ga_{As} *might* possess donor states.

The following evidence from the results confirms the existence of these donor levels for Ga_{As}. The donor level spacings in the different simulation contexts almost exactly match. The first (0/+) donor level is found 0.16 ± 0.01 eV below the $(-/0)$, and the second $(+/2+)$ donor level is 0.14 ± 0.01 eV below the first donor level. Most notably, the 512-site supercell level spacings almost exactly match the 216-site results. If the positive charge states were fully delocalized VB states, the defect banding in the different sized cells should cause numerical difference between the two cell size calculations. The final evidence that the positive Ga antisite states exists is seen in the nearest neighbor bond distances presented in table 3. The Ga–Ga bonds are strongest in the $Ga_{As}(2-)$ charge state when the Ga–Ga bonds are all fully saturated with electrons. The Ga–Ga bonds are the shortest for $Ga_{As}(2-)$, being 2.329 Å for the LDA. The transition to the $Ga_{As}(1-)$ state removes an electron from the defect, this electron coming from the local Ga–Ga bonds more than from the network bonds, weakening this bond and causing it to lengthen by 0.035 Å. As additional electrons are removed, these nearest neighbor bonds continue to get longer, by 0.029 Å to the neutral state, another 0.024 Å to the positive state and a final 0.019 Å in going to the doubly positive defect. This impact on

[2] The FDSM method is most accurate for deep levels with localized states. For shallow (Rydberg-like) states whose charge transitions follow the CB or VB, the FDSM calculations are less reliable, and tend to overstate the distance to a band edge.

Table 3. The Ga–Ga bond distance in the gallium antisite defect as a function of charge state, in Å.

	Simulation context			
Charge	LDA-216	LDA-512	LDA-3d	PBE
$Ga_{As}(2-)$	2.329	2.329	2.344	2.389
$Ga_{As}(1-)$	2.364	2.364	2.373	2.430
$Ga_{As}(0)$	2.393	2.391	2.397	2.467
$Ga_{As}(1+)$	2.417	2.410	2.417	2.498
$Ga_{As}(2+)$	2.436	2.424	2.432	2.528

the local structure shows that the electrons being removed come from the Ga–Ga bonds (the defect), not from the delocalized network bonds (the VB).

The formation energy of $Ga_{As}(0)$ in the LDA-512 supercell is 0.05 eV larger than the 3.19 eV formation energy computed in the LDA-216 supercell. The LDA formation energy agrees well with previous results, 3.0 eV [9], 3.15 eV [67] and 3.12 eV [46] (all converted to the arsenic-rich limit), with an early Northrup and Zhang result being an outlier at 3.79 eV [45]. The gallium antisite results do not appear to have a sensitivity to the functional. The computed PBE neutral formation energy, 3.20 eV, is very close the LDA result, as are the computed energy levels.

Unlike the arsenic antisite, the immediate neighbors of the gallium antisite are all gallium atoms, and replacement of the 3d-core PP with a 3d-valence PP has a more significant effect on the formation energy, which takes a lower value of 2.80 eV. The computed energy levels, however, are mostly unchanged (to within 0.1 eV) upon the substitution of the 3d-valence PP, despite an almost 0.4 eV change in the neutral defect formation energy. The energy levels, differences of total energies, are less sensitive to changes than the formation energies from which they derive; a theoretically convenient cancellation of differences appears to be taking place that renders calculation of defect energy levels more reliable than formation energies.

3.3. The double antisite, aa

An exchange of nearest neighbor As and Ga atoms results in a double-antisite defect. The bond network is unbroken and, with no change in the overall stoichiometry, the electrons in the neutral defect exactly fill all the bonds. In all the simulation contexts, the *aa* defect has no defect levels in the gap. The two extra valence electrons on the arsenic antisite compensate the two missing valence electrons on the neighboring gallium antisite. On the As_{Ga} side of the double antisite, we investigated distortions along As–As bonds similar to the distorted metastable state of the neutral isolated arsenic anitsite. No distorted local minimum was found in either the neutral charge state, or in a double negative charge state that would fill and stabilize the As lone pairs resulting from a breaking of the As–As bond in a As_{Ga}-like distortion.

The formation energy is similar in all simulations contexts. The LDA formation energy is 2.53 eV, the LDA-3d slightly smaller at 2.26 eV and the PBE formation energy of 2.44 eV almost exactly matches the LDA value. The 512-site formation energy differs from the 216-site value by less than 0.01 eV. The double antisite is strongly bound with respect to isolated (neutral) antisites; in fact, it has a smaller formation energy than the isolated neutral gallium antisite. The formation energy of *aa* is large enough that the defect concentration should be modest in the as-grown material, having populations competitive to the isolated antisite defects only in semi-insulating GaAs with a Fermi level near midgap. In radiation-damaged GaAs, the *aa* could potentially be created in greater numbers, but would be undetectable in any electrical

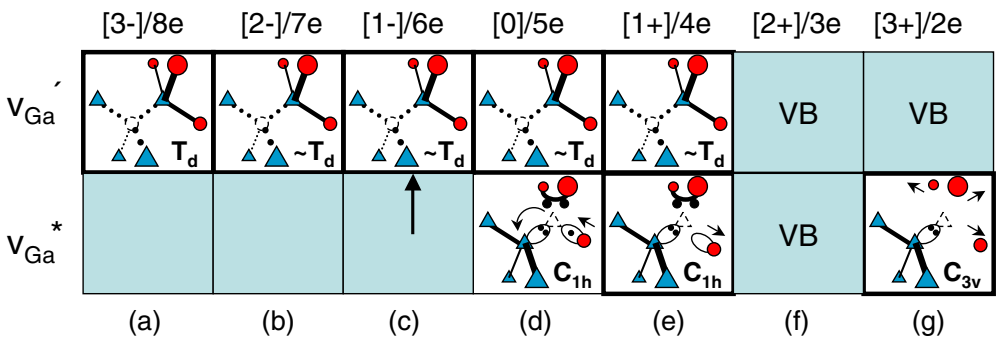

Figure 4. Schematic depiction of the ground state structures of the gallium vacancy, as a function of charge state or, equivalently, the valence electrons in the vacancy, ranging from (*a*) $v_{\mathrm{Ga}}(3-)$ to (*g*) $v_{\mathrm{Ga}}(3+)$. The (blue) triangles represent arsenic atoms and the (red) circles represent gallium. The simple gallium vacancy, v'_{Ga}, with approximately T_d symmetry, is stable from (3−) to (1+). For the (*d*) neutral vacancy, an adjacent As atom can into the Ga vacant site, forming v^*_{Ga}. Two of Ga atoms form a bond pair, reducing the symmetry to C_{1h}. This structure becomes the ground state for (*e*) $v_{\mathrm{Ga}}(1+)$, There is no stable (*f*) $v_{\mathrm{Ga}}(2+)$ structure. The (*g*) $v^*_{\mathrm{Ga}}(3+)$ loses both electrons of the Ga–Ga bond pair, all three trivalent gallium retreat from the vacancy, leaving the two remaining vacancy valence electrons in the As lone pair, converting $v^*_{\mathrm{Ga}}(3+)$ to the ideal C_{3v} symmetry. (Color online.)

measurement. However, radiation-induced antistructure pairs that are not nearest neighbors do have greater electrical activity [68].

3.4. The Ga vacancy, v_{Ga}

The removal of a gallium from the lattice results in a simple gallium vacancy: four adjacent arsenic atoms with lone pairs pointing toward the vacated site. In the neutral charge state, three electrons, the atomic valence of the missing gallium atom, are needed to saturate all the vacancy orbitals, limiting the maximum charge to (3−). Baraff and Schlüter first proposed that the gallium vacancy was not so simple, that v_{Ga} could be structurally bistable as a function of charge state [69], a result that was better quantified later by Pöykkö *et al* [70]. Our calculations confirm this qualitative picture: the gallium vacancy v_{Ga} takes both the form of a single gallium vacancy, which we label v'_{Ga}, and a form where a neighboring arsenic atom shifts in the vacant gallium site, creating a nearest neighbor As vacancy–As antisite pair we designate v^*_{Ga}, as illustrated in figure 4.

In agreement with previous calculations [8, 11, 45, 47, 60, 71], we find that v'_{Ga} takes negative charge states up to $v'_{\mathrm{Ga}}(3-)$. The earlier results for the Ga vacancy levels could be roughly divided into two camps [11]: those where all the levels were rather shallow or, as in the very first calculations of v_{Ga} levels by Baraff and Schlüter [8], relatively deep, with the $(3-/2-)$ level close to midgap. Our calculations support the second camp: the $v_{\mathrm{Ga}}(3-/2-)$ level at roughly midgap, $E_{\mathrm{v}} + 0.80(\pm 0.01)$ eV in all simulation contexts, the $v_{\mathrm{Ga}}(2-/1-)$ level in LDA is 0.16 eV lower, and the $v_{\mathrm{Ga}}(1-/0)$ level 0.16 eV lower yet. The PBE results are within 0.01 eV of the LDA results, a change in functional does not affect the acceptor states of v_{Ga}. The LDA-3d levels also show only small changes from the LDA calculations, indicating the result is insensitive to the Ga PP. In addition to what previous studies had predicted, our calculations indicate that a positive charge state is also possible. The v'_{Ga} can take all charges in the full range from (3−) to (1+). However, for positively charged v_{Ga}, the site-shifted v^*_{Ga} becomes important.

Despite electronic degeneracies, none of the $v'_{\rm Ga}$ charge state configurations manifest a detectable Jahn–Teller distortion. The structures retain the T_d symmetry of the ideal defect, with the adjacent As atom relaxing inward toward the vacant site from the ideal bulk positions. The variation in the structure as a function of charge state is even less than noted previously [11]. In our LDA simulations, the As atoms relaxed inward symmetrically by 12.9–14.2% as the charge on the defect changed from $v'_{\rm Ga}(1+)$ to $v'_{\rm Ga}(3-)$. The 3d-valence results were nearly the same, with an inward relaxation of 13.8%, for $v'_{\rm Ga}(1+)$, to 14.7%, for $v'_{\rm Ga}(3-)$. The PBE was not much different, with 11.1–12.8% inward relaxation.

The lack of detectable symmetry breaking indicates that the As atom bonds to the network dominate the weaker As–As interactions across the vacancy. Each three-fold As atom forms an acute pyramid to emphasize the s-like character in the As lone pair and the p-like character in the bond orbitals to its remaining Ga neighbors. The As atoms around the vacancy have pyramid angles much reduced from the tetrahedral 109.5°. In LDA, for example, angle ranges from 102.3° for the $v'_{\rm Ga}(1+)$ to 100.8° for the $v'_{\rm Ga}(3-)$. Reflected in the deep acceptor levels in the gap, these pyramidal arsenic atoms with lone pairs are very stable. This is a structural motif seen repeatedly in many different GaAs defects.

The site-shifted form of the vacancy, $v^*_{\rm Ga}$, can take charge states from neutral to (3+). The structure of $v^*_{\rm Ga}$ is more variable than $v'_{\rm Ga}$, having internal bistabilities in addition to the global bistability with $v'_{\rm Ga}$. The ideal defect has a C_{3v} symmetry, with one As atom and three Ga atoms surrounding the vacancy. The (3+) charge state, figure 4(*g*), does take the C_{3v} symmetry. However, all other charge states prefer to form a Ga–Ga bond pair across the vacancy and reduce the symmetry to C_{1h}. As illustrated in figure 4, the $v^*_{\rm Ga}$ passes through a sequence of bonding configurations as it progresses from the neutral to the (3+) state.

The five electrons of $v^*_{\rm Ga}(0)$ distribute themselves into a lone pair on the arsenic, a Ga–Ga bond pair and one electron in the dangling bond on the remaining Ga. All adjacent atoms contract inward from ideal, the Ga–Ga in order to form a bond pair, the As to stabilize the three-fold pyramidal bonding (as in the $v'_{\rm Ga}$) and the remaining Ga also forms a three-fold pyramid, driven by a partially occupied lone pair. The Ga–Ga bond distance in $v^*_{\rm Ga}(0)$ is 2.85 Å in LDA and 3.00 Å in PBE. Removal of an electron to form $v^*_{\rm Ga}(1+)$ causes the unpaired Ga to retreat from the vacancy, by ∼0.6 Å from its position in $v^*_{\rm Ga}(0)$, flattening the pyramid, toward an sp^2-hybridized planar structure characteristic of trivalent Ga. The Ga–Ga pair and As lone pair left behind are mostly unchanged. The computed $v_{\rm Ga}(2+)$ structure is almost identical to the $v_{\rm Ga}(1+)$. The $v_{\rm Ga}(2+)$ charge state is (partially) entangled in the VB, the As lone pair unwilling to give up a full electron and leave behind a positively charged As and the Ga–Ga pair also being below the VB edge. The calculation does not represent a true $v^*_{\rm Ga}(2+)$ defect state, but is a computational artifact corresponding to $v^*_{\rm Ga}(1+)$ plus a VB hole.

Removing an additional electron to form $v^*_{\rm Ga}(3+)$ state triggers another structural change and results in a true defect state. All Ga atoms become trivalent and retreat outwards. The Ga–Ga bond pair disappears, leaving the last two vacancy electrons in the As lone pair. The As atom has been mostly unaffected in this entire sequence of charge transitions, the action restricted to more agile Ga atoms. This sequence of bonding transitions with charge state in the $v^*_{\rm Ga}$ is observed in all simulation contexts. That the Ga atoms are more flexible in their bonding than the As is already reflected in the elemental bulk structures: elemental Ga has complex, variable bonding in the *A*11 structure [29] and the As uniformly has a simple pyramidal structure in the *A*7 [30]. The puckering of the trivalent Ga to a near-planar configuration is a second prominent structural motif that repeats in many GaAs defects. The Ga–Ga vacancy bond pair is a third prominent structural motif of GaAs defects, and the importance of this motif has significant numerical consequences for the simulations. In the Ga vacancy, the breaking

of the Ga–Ga bond results in a negative-U $v^*_{Ga}(1+/3+)$ system in all simulation contexts, a stronger negative-U than from the site shift between v'_{Ga} and v^*_{Ga}.

Unlike in the GaAs antisite defects, the functional and PP have a significant energetic consequences for the v_{Ga}, because of the Ga–Ga stretched bond pair. Constrained by the back bonds to the lattice network, the Ga–Ga bond in v^*_{Ga} is stretched from ideal, being $18(17) \pm 1\%$ larger than the bulk Ga–As distance in LDA(LDA-3d). The Ga–Ga bond in PBE is $21 \pm 1\%$ larger than the bulk Ga–As distance. The PBE typically does better in dissociating bonds than LDA. The dissociation curve is too steep in LDA, and stretching the Ga–Ga bond incurs a greater energy penalty than it should, and a greater penalty than in the PBE. The differential energy penalty changes the defect energy level spectrum, as PBE has a larger negative-U for $v_{Ga}(3+/1+)$, triggered by the bond-pair breaking, and creates a second negative-U $v_{Ga}(1\text{-}/1+)$ not present in the LDA, triggered by the site change.

Adding an electron to $v^*_{Ga}(0)$ causes the antisite-As atom to hop back to its original lattice site without a barrier, converting to the simple $v'_{Ga}(1-)$. The neutral vacancy strongly prefers the simple $v'_{Ga}(0)$ structure over the site-shifted $v^*_{Ga}(0)$ structure, by 0.59 eV in LDA. 0.67 eV in LDA-3d and 0.45 eV in PBE. The formation energy of the $v'_{Ga}(0)$ is 2.69 eV, 2.50 eV and 2.65 eV in the LDA, LDA-3d and PBE, respectively. This LDA formation energy (As-rich conditions) is significantly less than the 4.0 eV quoted in early DFT studies [9, 45], but is in general agreement with more recent values of 2.2 [60], 2.8 [47]. 2.47 [71], 2.65 [46] and 2.58 eV [11].

The choice of simulation context has more qualitative impact for $v_{Ga}(1+)$. The LDA favors $v'_{Ga}(1+)$ by 0.01 eV in the 216-site cell and $v^*_{Ga}(1+)$ by 0.04 eV in the 512-site cell, indicating good convergence with cell size, but the LDA-3d favors the simple v'_{Ga} by 0.17 eV. Hence, there is no (or minimal) relaxation gained from a site switch by $v_{Ga}(0/1+)$, and no negative-U in the LDA. The PBE functional does not incur a stretched-bond penalty for the Ga–Ga pair in $v^*_{Ga}(1+)$, and $v^*_{Ga}(1+)$ is more stable than $v'_{Ga}(1+)$ by 0.24 eV. This extra stabilization from the site change in PBE creates a negative-U $v_{Ga}(1 - /1+)$ system. In fact, this negative-U system is embedded inside the larger $v_{Ga}(1 + /3+)$ negative-U system, with the computed $(2 + /3+)$ transition being above both the $(1 - /0)$ and $(0/1+)$ transitions. The observation of overlapping negative-U systems within a single defect is a first of its kind. However, we reiterate that, because the $v^*_{Ga}(2+)$ state is contaminated by bulk bands, the values of the $(2+/q)$ levels are not numerically predictive, and this may be a computational artifact rather than real.

The gallium vacancy in GaAs has proven remarkably elusive experimentally, with the general consensus that whatever levels v_{Ga} has must lie below midgap. Our calculations identify charge states ranging from $(3-)$ to $(3+)$, with all the levels at midgap and below. A single experimental study has claimed to identify an electrical level due to v_{Ga} [57], assigning an acceptor state at $E_v + 0.042$ eV to v_{Ga}. The lowest acceptor state of v_{Ga} in our calculations, the $(1 - /0)$, is 0.5 eV above the VB edge, and v_{Ga} possesses three donor states below that level. Therefore it seems unlikely that this experimental assignment is correct.

3.5. The As vacancy, v_{As}

We find that arsenic vacancy, v_{As}, like v_{Ga} can take charge states ranging from $(3-)$ to $(3+)$. The interesting result for v_{As} is that it possesses a total of three negative-U systems, regardless of simulation context, the $(3 - /1-)$ level at 0.3–0.4 below the CB edge, the $(1 - /1+)$ level spanning midgap and a final $(1 + /3+)$ level near the VB. All odd-electron charge states of v_{As} are predicted to be thermodynamically unstable. The structures exhibit the same chemical bonding motifs identified in the gallium vacancy, as illustrated in figure 5.

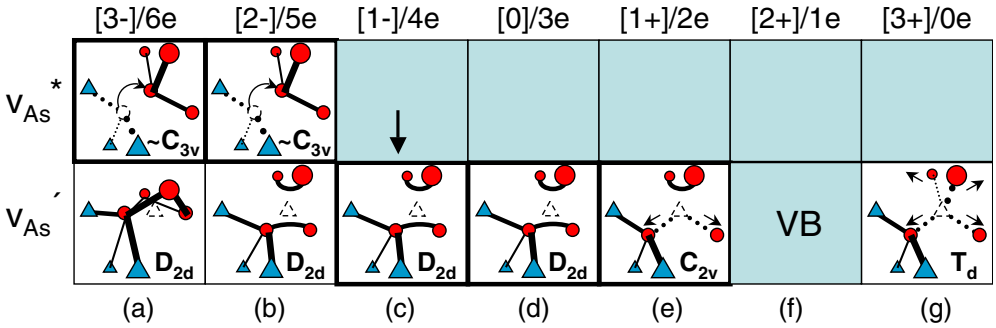

Figure 5. Schematic depiction of the ground state structures of the arsenic vacancy, as a function of charge state (valence electrons in the vacancy) ranging from (*a*) $v_{\rm As}(3-)$ to (*g*) $v_{\rm As}(3+)$. The (blue) triangles represent As, (red) circles, Ga. The site-shifted $v^*_{\rm As}$ takes $\sim C_{3v}$ symmetry, and is only stable in (3−) and (2−) states, it relaxes into the simply vacancy $v'_{\rm As}$ otherwise. The Ga atoms adjacent to the simple arsenic vacancy, $v'_{\rm As}$, take up different bonding as a function of the number of electrons in the vacancy, the number of Ga–Ga bonds present determining the symmetry of the defect, see text. (Color online.)

Like the gallium vacancy, $v_{\rm As}$ exhibits a site-shift bistability as a function of charge state, as first described by Baraff and Schlüter [72]. They predicted that $v^*_{\rm As}$ would have four charge states, ranging from (3−) to (1+). Including full relaxation in larger cells, we find that $v'_{\rm As}$ can take charge states from (3−) to (3+), and that the site-shifted $v^*_{\rm As}$ is only able to take (3−) and (2−) charge states. Constrained to C_{3v} symmetry, the Ga atom in the site-shifted $v^*_{\rm As}(1-)$ takes up a position near midway between the Ga and As sites in a 'split-vacancy' configuration, but relaxes fully to $v'_{\rm As}(1-)$ when the symmetry is reduced to C_{1h}.

The negatively charged (3−) and (2−) states, figure 5(*a*) and (*b*), prefer the site-shifted $v^*_{\rm As}$, with three As atoms adjacent to the vacancy having lone pairs that readily take up additional electrons. The $v_{\rm As}(3-/1-)$ negative-U transition is triggered by this site-shift between $v^*_{\rm As}(2-)$ and $v'_{\rm As}(1-)$.

The $v'_{\rm As}(1-)$, figure 5(*c*), has four electrons in the vacancy to distribute among the four Ga atoms adjacent to the vacancy. These form two Ga–Ga bond pairs (2.74 Å in LDA, 2.86 Å in PBE) in a D_{2d} symmetry in the same manner as the neutral vacancy in silicon, adopting the same structural motif seen in the $v'_{\rm Ga}$ structures. The strong-pairing D_{2d} structure for the $v'_{\rm As}(2-)$ and $v'_{\rm As}(1-)$ was first reported by Laasonen, *et al* [73], and reproduced in more recent studies [11, 74]. Adding an electron, the $v'_{\rm As}(2-)$ preserves the D_{2d} symmetry of the $v'_{\rm As}(1-)$, but is only metastable, being slightly (0.03 eV in LDA and 0.04 eV in PBE) less stable than $v^*_{\rm As}(2-)$. The $v'_{\rm As}(3-)$ undergoes a Jahn–Teller distortion into a resonant-D_{2d} structure [11], but is significantly less stable (0.3–0.4 eV) than the site-shifted $v^*_{\rm As}$. An experimental measurement of the $(3-/1-)$ may find itself trapped in $v'_{\rm As}$ as it takes up electrons, conversion from $v'_{\rm As}$ to $v^*_{\rm As}$ involves a more significant barrier (unlike the reverse transition). A trapped $v'_{\rm As}(3-/1-)$ is also negative-U, in LDA and PBE, by 0.2 ± 0.1 eV, a result that will become important in attempting to assign defects to observed experimental levels later.

The D_{2d} structure is preserved in the (three-electron) $v'_{\rm As}(0)$, although the stretched Ga–Ga bonds stretch even further when an electron is missing. Removing an additional electron leaves only two valence electrons in $v'_{\rm As}(1+)$. The two vacancy electrons would fill the symmetric a orbital in a T_d structure, and, lacking an electronic degeneracy to drive a Jahn–Teller distortion, suggests a T_d ground state for the defect. However, we find the two electrons prefer to keep one

of the Ga–Ga bonds from the D_{2d} structure, causing the other unpaired, trivalent Ga atoms to retreat outwards, leaving a C_{2v}-symmetry vacancy, as illustrated in figure 5(*e*). This preference for a Ga–Ga bond is small, less than 0.1 eV, but apparently real, being present in all simulation contexts. The lattice relaxation of breaking a Ga–Ga bond pair in going to $v'_{\rm As}(1+)$ causes the second negative-U transition $v_{\rm As}(1+/1-)$. As in $v_{\rm Ga}$, the energetics of the stretched bond pair are sensitive to functional, and, while LDA does predict a negative-U here, the PBE negative-U is wider, with the interesting consequence that its two upper negative-U systems overlap each another.

Notwithstanding that the $v'_{\rm As}(2+)$ is embedded in the valance band (LDA), or very close (PBE), we find that $v_{\rm As}(1+)$ is not the last positive charge state, unlike previous work [11, 67, 75, 76]. A third negative-U system $v_{\rm As}(1+/3+)$ is caused by yet another structural change: the $v'_{\rm As}(3+)$ has no valence electrons remaining in the vacancy. The last Ga–Ga bond pair disappears, and all the adjacent Ga atoms retreat strongly outward to more planar, trivalent positions. The ground state $v'_{\rm Ga}(3+)$ takes a T_d symmetry, figure 5(*g*). We find the $(1+/3+)$ negative-U level at less than 0.1 eV above the VB edge for all the LDA calculations, It is deeper in the gap, at $E_v + 0.28$ eV, for PBE. Once more, the Ga–Ga stretched bond energy is sensitive to functional, and PBE is likely to be the more accurate description of the breaking of this bond. Stable in every simulation context, the (3+) charge state is likely to be real and not computational artifact. Our calculation confirms the stability of the $v_{\rm As}(3+)$ first proposed by Northrup and Zhang [77], but apparently not reproduced in published work since.

The LDA formation energy of $v_{\rm As}$ is 3.55 eV, in good agreement with other recent calculations of 3.60 [46] and 3.61 eV [11]. The better consistency between different theoretical calculations (as compared with the greater scatter among the $v_{\rm Ga}(0)$ reported results above) is probably due to better convergence with cell size in these more recent studies. The formation energy is insensitive to the cell size, the LDA-512 formation energy that is only 0.01 eV lower than the 216-site supercell value. There is only modest sensitivity to functional and PP. The PBE formation energy, 3.44 eV, and the LDA-3d, 3.41 eV, are less than 0.2 eV smaller than LDA.

In contrast to the neutral formation energies, the differences in computed defect levels from previous results [11, 73, 75, 77] is much greater. We obtain reliable $v_{\rm As}$ defect energy levels for the full range of charge states available to $v_{\rm As}$, (3+) to (3−), including the site-shifted $v^*_{\rm As}$. And differences for individual transitions with the simple $v'_{\rm As}$ are probably due to the use of fully relaxed structures in well-converged supercells and the use of the FDSM to control the charge boundary conditions.

3.6. The divacancy, vv

The divacancy in GaAs has not been extensively studied. An early calculation due to North and Zhang [77] computed a large formation energy for $vv(0)$ of 4.8 eV, and concluded that the divacancy would be nonexistent in equilibrium conditions. A different study [76] found a smaller value, 3.54 eV, but still large enough to preclude significant concentrations of vv in equilibrium GaAs. The vv could potentially be of interest in radiation-damaged GaAs. Puska and Corbel [78] did early calculations of vv structures and positron lifetime, and reported that the vv atoms relaxed outward, with an increased lifetime of the positron of 320 ps (compare with a bulk calculated value of 229 ps). Positron annihilation experiments in irradiated GaAs have cited the absence of a lifetime this long to reject the existence of vv [79]. Improved DFT calculations predicted modest inward relaxations within vv [76], not large enough to overturn the original conclusion. Rare in equilibrium GaAs and reportedly unobserved in irradiated GaAs, the vv in GaAs has been largely ignored in computational studies.

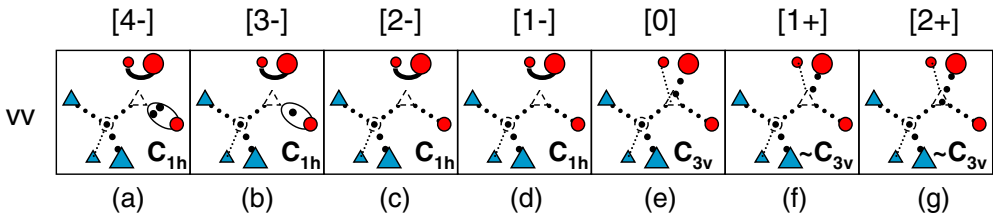

Figure 6. Schematic depiction of the ground state structures of the divacancy, as a function of charge state. The divacancy takes charge states ranging from (*a*) $vv(4-)$ to (*g*) $vv(2+)$. For (*g*) $vv(2+)$ through (*e*) $vv(0)$, all the vacancy valence electrons populate the As lone pairs on the v_{Ga} side of the vacancy. The strongly pyramidal As atoms relax strongly inward and the Ga trivalent relax outward from the vacancy, resulting in an approximate C_{3v} symmetry. Starting with (*d*) $vv(1-)$, a Ga–Ga bond pair forms on the v_{As} side of the divacancy, reducing the symmetry to C_{1h}. The remaining Ga atom captures first one, and then a second electron in its lone pair in (*b*) $vv(3-)$ and (*a*) $vv(4-)$, causing it to pucker in toward the vacant site. (Color online.)

The divacancy plays a much more important role in GaAs than these early studies indicated. We find the divacancy can take charge states from (2+) to (4−), with transitions across almost the entire band gap. The earlier DFT study [76] had predicted only three charge states, with relatively shallow levels of $vv(2-/1-)$ at $E_v + 0.19$ and $vv(1-/)$ at $E_v + 0.12$ (and the $vv(0/+)$ just below the VB). The smaller 64-site supercells with Γ-point sampling that were computationally tractable at the time are simply inadequate to describe defects in GaAs.

The vv defects take structures that adhere to the rules described by the same structural motifs identified in the monovacancies, as illustrated in figure 6, irrespective of the simulation context. Unlike the monovacancies, the vv does not have a site-shift bistability. The bonding in vv is most conveniently described in terms of its two components: a v_{Ga} with three adjacent As atoms and a v_{As} with three adjacent Ga atoms, that do not structurally interact, and into which integral numbers of electrons are placed. As in the v'_{Ga} monovacancy, the As atoms on the v_{Ga} side of the divacancy all pucker strongly inward and show minimal distortions from an ideal local C_{3v} symmetry regardless of the charge state. As in v'_{As}, the Ga atoms on the v_{As} side of the divacancy vary their bonding as electrons are added.

There are six valence electrons in the neutral divacancy. In the ground state C_{3v} structure, the three As lone pairs on the v_{Ga} side take up all of the vacancy electrons, leaving the Ga lone pairs on the v_{As} side unoccupied, and the trivalent Ga all relax strongly outward. We found two metastable structures, both corresponding to shifting two electrons to the v_{Ga} side: a C_{1h} structure with a Ga–Ga bond pair, 0.27–0.30 eV higher in the LDA calculations and 0.65 eV higher in the PBE, and a second C_{3v} structure with the Ga atoms puckered inward, higher yet by 0.1 eV. The $vv(0)$ formation energy of 4.19 eV in LDA and 3.59 eV in PBE are comparable to the computed $v_{As}(0)$ formation energy. The divacancy is strongly bound against dissociation into the monovacancies. Each As dangling bond ideally contains $\frac{5}{4}$ electrons and the Ga dangling bond $\frac{3}{4}$ electrons. The ground state of $vv(0)$ is strongly dipolar, with $\frac{9}{4}$ electrons shifted from the v_{As} side to the v_{Ga} side in comparison to an ideal, unpolarized divacancy. We find that up to two electrons can be removed from $vv(0)$ before there are no more occupied gap states. The $vv(1+)$ and $vv(2+)$ structures do not change much from $vv(0)$, remaining $\sim C_{3v}$. These positive divacancies, like $vv(0)$, have metastable structure shifting two electrons to the v_{As} side, both with roughly the same relative energy as in $vv(0)$.

The $vv(1-)$ takes a C_{1h} ground state, as one electron gets pulled from As lone pairs on the v_{Ga} side of the defect to form a Ga–Ga bond pair in the v_{As} side, illustrated in figure 6. This bond pair endures through all the negatively charged states. The lattice relaxation involved in

breaking of this bond pair causes the $vv(2-/0)$ negative-U system. Adding an electron to form $vv(2-)$ refills the hole in the As lone pairs, leaving the overall structure mostly unchanged from $vv(1-)$. The next electron, to form $vv(3-)$ finds the last Ga atom, partially filling its lone pair, causing it to pucker inward by 0.6–0.7 Å from the trivalent near-planar configuration in the $vv(2-)$ state. The vv accommodates yet another electron in the gap, which also is deposited onto this Ga lone pair, causing it to pucker even further inward, by 0.2–0.3 Å, retaining a C_{1h} symmetry for the ultimate $vv(4-)$ charge state. The As atoms are all within 2.1–2.2 Å of the central vacant Ga site, and the Ga atoms are all within 1.85 (LDA) to 1.97 (PBE) Å of the center of the As vacant site.

3.7. The Ga interstitial, Ga_i

Interstitials in semiconductors are exceedingly elusive, with few if any isolated interstitials directly identified in any semiconductor [3]. Their presence and activity is inferred through changes in defect chemistry. Interstitial-impurity complexes appear or vacancies disappear as an irradiated material is annealed, implying that interstitials are mobile species in GaAs and other semiconductors. While the gallium interstitial Ga_i in GaAs has never been directly observed, the diffusion of gallium interstitials in GaAs has been probed using zinc diffusion experiments. One experimental analysis implicated $Ga_i(2+)$ and $Ga_i(3+)$, with perhaps a small contribution from $Ga_i(1+)$, as the mobile species. [80] A later experiment disputed this, asserting that the mobile charges states were $Ga_i(1+)$ and $Ga_i(0)$ [81]. The available modeling for the gallium interstitial is no more harmonious [8, 82–87], with no two sets of results in substantive agreement with one another. The most recent, due to Malouin and co-workers [86], used the most converged theory, and describes a very complex chemistry of charge states ranging from $(3-)$ to $(1+)$.

Surprisingly, we find the best qualitative agreement with the earliest, presumably most primitive predictions. Baraff and Schlüter [8], using Green's function techniques and unrelaxed geometries, predicted the tetrahedral interstitial site with gallium neighbors, which we label $T_{i,g}$, would be singly ionized across the band gap, and the ground state for $Ga_i(1+)$, while the $T_{i,a}$ would range from singly ionized to triply ionized, with a $(1 + /2+)$ transition near $E_v + 0.51$ eV and a $(3 + /2+)$ transition near +0.15 eV. Our calculations confirm this general picture. The only thermodynamically stable states we find are positively charged defects, in tetrahedral interstitial configurations.

The $T_{i,g}$ site, figure 7(*b*), is the ground state structure for $Ga_i(1+)$. It has no levels in the gap. The $T_{i,a}$ is 0.27 eV (0.19/PBE,0.21/LDA-3d) higher in energy and has two donor levels. The first $(1 + /2+)$ donor level of $T_{i,a}$ is 0.2–0.3 eV above the VB, the second $(2 + /3+)$ donor level is shallow, within 0.1 eV of the VB (it is these transitions which are presented in figures 1 and 2). The $T_{i,a}(2+)$ and $T_{i,a}(3+)$ are the lowest energy configurations of Ga_i for those charge states. Positively charged tetrahedral interstitials all have full tetrahedral symmetry, attempted distortions all return to the T_d-symmetric site.

Our calculations predict diffusion of Ga_i involves a migration barrier of $\gtrsim$1 eV. The $Ga_i(1+)$ migration barrier between the $T_{i,g}$ ground state and $T_{i,a}$ structure through the non-bonded C_{3v} 'hexagonal' channels (designated as an H site) is not sensitive to functional. The computed barrier through a non-bonded H site is 1.22 eV in LDA and 1.11 eV in PBE. Alternatively, diffusion could proceed through insertion into the lattice network. All in-network configurations for $Ga_i(1+)$ collapse to one of these three structures: a C_{2v} 110_g-split interstitial, a D_{2d} $0\,0\,1_g$-split interstitial, and a C_{3v} bond-centered B_C structure, illustrated in figure 7(*c*)–(*e*). The lowest energy in-network structure is B_C, where the divalent Ga_i forms two bonds with its neighbors, at 0.95(0.83) eV above the $T_{i,g}$ site using LDA(PBE). This is in quantitative

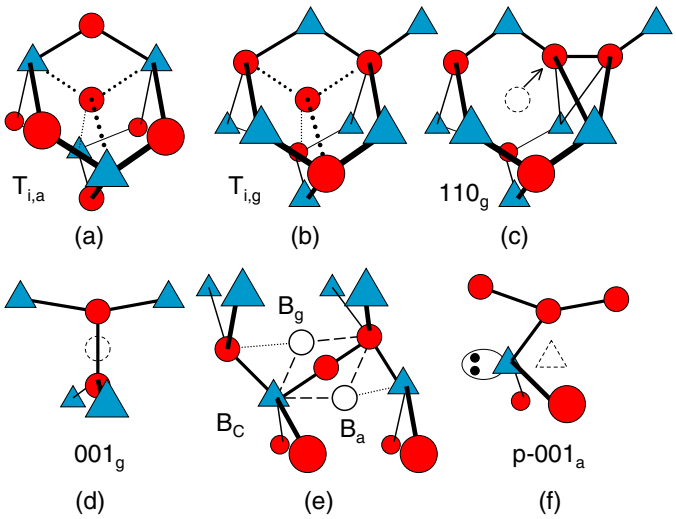

Figure 7. Schematic depiction of the interesting structures for the Ga_i. (*a*) $T_{i,a}$ structure: Ga_i sitting in a non-bonded tetrahedal interstice with As neighbors. (*b*) $T_{i,g}$ structure: Ga_i sitting in the other non-bonded tetrahedral interstice with Ga neighbors. (c) The C_{2v} symmetry 110_g-split interstitial. (*d*) The D_{2d} symmetry 001_g-split interstitial. (*e*) Bond-bridging structures: the C_{3v} bond center B_C, or bent-bridge B_g and B_a structures with the interstitial shifted toward the $T_{i,g}$ or $T_{i,a}$ side of the bond. (*f*) p-001_a: a puckered 001_a split interstitial, puckered to accommodate a pyramidal As with a full lone pair and planar trivalent Ga atom. (Color online.)

agreement with earlier results [86, 87]. They went further to evaluate a 0.4 eV barrier to hop from the B_C site (which they labeled a 1 1 1-split $_{[Ga–As]}$) to the tetrahedral site, reporting a total $T_{i,g}$–$T_{i,g}$ migration barrier of 1.3 eV. We find the 1 1 0_g structure is next, at 1.12(1.07) eV above the $T_{i,g}$, and 0 0 1_g structure is last, at 1.29(1.34) eV above the $T_{i,g}$ structure using LDA(PBE). The energy barrier from these defects to the $T_{i,g}$ was not computed for these charge states, but is expected to be on the order of a few tenths of an electronvolt, leading to barriers slightly higher than the off-network path through the *H* site. The dominant migration path for $Ga_i(1+)$ will likely be along a non-network path, with some small contribution from in-network paths.

The migration barriers for the (2+) and (3+) charge states will be comparable to or perhaps slightly higher than the barrier for the (1+) charge states. With the disappearance of the $T_{i,g}(2+)$ state into the VB, the migration must be through an in-network path. The 1 1 0_g-split interstitial is 0.9–1.0 eV higher than the $T_{i,a}$ for these charge states, similar to the energy for inserting into the network for Ga_i. The 0 0 1_g is another 0.2–0.3 eV higher than the 1 1 0_g structure. We found no other stable structures for the $Ga_i(2+)$ or $Ga_i(3+)$. The result that the (1+), (2+), (3+) structures all have similar migration barriers suggests that they should have similar diffusion rates (a detailed analysis of diffusion lies outside the scope of this paper).

The existence and mobility of $Ga_i(1+, 2+, 3+)$ agree with the original analysis of Bösker *et al* [80], and conflicts with the later reassessment of Bracht and Brotzmann predicting diffusion via $Ga_i(1+)$ and $Ga_i(0)$ [81]. Not only do our results indicate the positive defects should have similar migration energies, but we predict that $Ga_i(0)$ is not even a thermodynamically stable charge state. The $Ga_i(0)$ cannot contribute significantly to diffusion. In light of these new results, we suggest that the diffusion of Ga interstitials in GaAs needs to be revisited.

The neutral and negative Ga_i pose interesting exercises in computational analysis of defect calculations. In a computational survey of all plausible $Ga_i(0)$ structures, the $T_{i,g}(0)$ calculation

Table 4. Characteristic distances in Ga_i as a function of charge state, in Å (LDA).

	Defect structure, signature distance			
Charge state	$T_{i,g}$ $R(Ga_i–Ga)$	$T_{i,a}$ $R(Ga_i–As)$	$1\,1\,0_g$ R(Ga–Ga)	$0\,0\,1_g$ R(Ga–Ga)
$Ga_i(1-)$	2.597	2.541	2.821	2.220
$Ga_i(0)$	2.599	2.541	2.736	2.220
$Ga_i(1+)$	2.602	2.540	2.647	2.218
$Ga_i(2+)$	2.603	2.501	2.599	2.313
$Ga_i(3+)$	2.604	2.467	2.571	2.501

emerges with the lowest energy, and the $T_{i,a}(0)$ is higher by 0.2–0.3 eV. The in-network neutral structures are led by $1\,1\,0_g$, at 0.6–0.7 eV above the $T_{i,g}$. Bond-center-derived structures are next, where the Ga becomes trivalent and buckles the bond, as depicted in figure 7(*e*). Buckling the B_C structure in the $[0\,0\,\bar{1}]$-direction (toward a [1 1 0]-direction with the As atom), the B_a remains two-fold coordinated and forms a bridge bond between the network As and Ga atoms. Buckled in the [0 0 1]-direction (toward a [0 0 1]-direction with the As atom), the B_g structure relaxes through the bridge bond: the interstitial Ga atom inserts itself into a second As–Ga bond and leaves the As three-fold coordinated. This structure, depicted in figure 7(*f*), has the bond connectivity of a $0\,0\,1_a$ split interstitial: a Ga sharing an As site, split along the [0 0 1]-direction, the As puckered out of its plane, reducing the symmetry of the $0\,0\,1_a$ split from the ideal C_{2v} to C_{1h}. Two prominent structural motifs, a pyramidal As, with a full lone pair, and the trivalent Ga have appeared amongst the interstitial structures. Respecting the connectivity, we designate this structure as p-$0\,0\,1_a$ (in previous work [86] this had been labeled 1 1 0-split[Ga–As]). The two bond-bridge-derived structures are roughly equal, both 0.9 eV above the $T_{i,g}$ energy. The $0\,0\,1_g$ split interstitial is the final structure, much less stable at 1.4–1.6 eV higher than the computed $T_{i,g}$ energy. Superficially, the gallery of $Ga_i(0)$ defects is the same as for $Ga_i(1+)$, with a similar order.

Examined more closely, we find that the lowest energy $Ga_i(0)$ supercell calculations, the T_i structures, are not true defect states, both place an electron into the CB. The network bond topology for the T_i interstitials is unchanged from the perfect crystal, and there is close correspondence between the KS eigenvalues of the perfect crystal supercell and the defected supercell. A simple inspection reveals that the newly occupied level is a CB state, not a defect state in the gap. The defect state is several tenths of electronvolts above the CB edge. If it were a defect state, the electron would be derived from a p orbital on the interstitial gallium, with an orbital degeneracy that should trigger a Jahn–Teller distortion. All symmetry-lowering distortions of the Ga_i in the tetrahedral site relaxed back to the high-symmetry position. A NEB calculation connecting the $T_{i,g}$ configuration with the $1\,1\,0_g$-split interstitial (a true defect state) showed that the occupied KS state in the gap for the $1\,1\,0_g$ geometry rose and crossed the apparent CB edge very close to the $1\,1\,0_g$ configuration.

A final check is to examine the behavior of a characteristic bond distance in the defect as a function of charge state, as presented in table 4. The Ga_i–Ga distance around the $T_{i,g}$ interstitial does not change for any charge state from (1−) to (3+), consistent with no localization of an electron with any change in charge state. Only the $T_{i,g}(1+)$ is a true defect state. The Ga_i–As distance in the $T_{i,a}$ configuration changes as the defect steps from (1+) to (2+), and from (2+) to (3+), signaling a change in occupation of a localized defect state, but the (0) and (1−) charge states have the same distances as the (1+) charge defect, indicating electrons occupied delocalized band states rather than a localized defect state. The central Ga–Ga distance in the

$1\,1\,0_g$ structure changes with every change in charge state, starting at 2.82 Å for the (1−) charge and decreasing to 2.60 Å for the (3+) charge state. The central Ga–Ga distance in the $0\,0\,1_g$ indicates the neutral and negative charge states are CB states rather than valid defect states. These observations are consistent with the inferences made by comparing the KS eigenvalues of the defect calculations to the crystal supercell calculations. The consistency of the KS spectrum and bond analysis to identify a defect state in Ga_i adds support to the earlier analysis predicting gallium antisite would have two donor levels based mostly on the bond analysis alone.

In-network structures, the $1\,1\,0_g$-split and the bond-bridge structures, are the only true defect states for $Ga_i(0)$, with the $1\,1\,0_g$ structure having the lowest energy. The neutral interstitial is thermodynamically unstable, it is exothermic to emit an electron to the CB and form the $T_{i,g}$. A large lattice relaxation of ∼1 eV from the $1\,1\,0_g$ in-network structure to the tetrahedral interstitial is responsible. An NEB calculation finds (almost) no barrier for $Ga_i(0)$ in the $1\,1\,0_g$ structure to convert to the $T_{i,g}$, the reverse of the process shown in figure 7, the $1\,1\,0_g$ structure is not even a minimum. There is only a very small range of neutral configurations around the $1\,1\,0_g$ (and the bridge-bond) structures that are defect states, small islands of stability in what is mostly a sea of computational artifacts that actually describe a positive defect plus a conduction electron. The large $Ga_i(0)$ formation energy reflects this lack of stability, being 4.26(4.20) eV in LDA and PBE (in the ground state $1\,1\,0_g$ structure). The LDA-3d result is slightly lower, at 4.10 eV.

The neutral in-network structures each have a negative charge defect state, which appears to be more stable than the neutral, compared with the tetrahedral non-bonded site. For example, the $1\,1\,0_g$ $Ga_i(1-)$ has a more significant barrier (0.4 eV) against shifting to $T_{i,g}$, indicating a greater range of stability. If the $Ga_i(1-)$ were truly a valid defect state and form a negative-U $(1-/1+)$, the calculations show the level would be within 0.03 eV of the CB. Given the large lattice relaxation that would be required, and the lack of any stable intermediate neutral state, we deem this unlikely, and conclude that the Ga interstitial in GaAs can appear only as a positively charged defect.

3.8. The As interstitial, As_i

We find the arsenic interstitial takes charge states ranging from (1−) through (3+). The As interstitial exhibits an extreme multistability, almost every change in charge state leads to a different ground state structure, many with relatively low-energy competitive structures. A schematic depiction of the competitive structures for As_i is presented in figure 8. The As_i has a global bistability between off-network and in-network configurations: the highly ionized As_i prefers non-bonded interstitial sites, the As_i with more electrons prefer to use those electrons to form bonds within the lattice. The relative energetics of the different structures are presented in table 5.

The $As_i(3+)$ is a stable defect that sits in the tetrahedral interstices, $T_{i,a}$ and $T_{i,g}$ with full T_d symmetry. These sites are within 0.1 eV of each other, LDA slightly prefers $T_{i,a}$ and PBE favors the $T_{i,g}$ site. A C_{3v} symmetry H site, the (approximately) hexagonal window between T_i sites, is a saddle point between these two T_i, with a barrier of only 0.3–0.4 eV. However, the state of this H (3+) barrier configuration is contaminated with the VB, and hence this calculation may slightly underestimate a true DFT barrier for migration.

The $As_i(2+)$ inserts an As atom with a s^2p^1 atomic configuration. With the resulting p-like orbital degeneracy, the T_i sites undergo Jahn–Teller distortions. An H site in the channel becomes the ground state within the non-bonded interstices. The tetrahedral sites are 0.2 eV

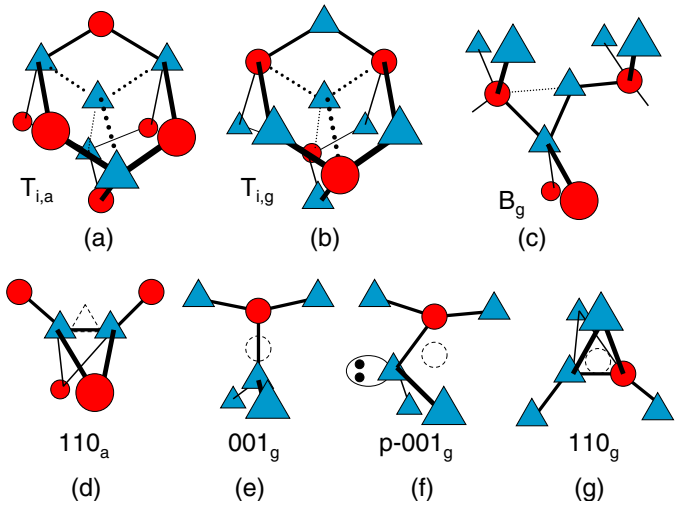

Figure 8. Schematic depiction of the low-energy structures for As_i. (*a*) $T_{i,a}$ structure: As_i sitting in a non-bonded tetrahedral interstice with As neighbors. (*b*) $T_{i,g}$ structure: As_i sitting in the other non-bonded tetrahedral interstice with Ga neighbors. (*c*) B_g bent bond structure, bent toward the $T_{i,g}$ site. (*d*) The C_{2v}-symmetry $1\,1\,0_a$-split interstitial. (*e*) The C_{2v}-symmetry $0\,0\,1_g$-split interstitial. (*f*) The C_{1h}-symmetry, puckered-$0\,0\,1_g$-split interstitial, with a pyramidal As and planar Ga atom. (*g*) A C_{1h}-symmetry $1\,1\,0_g$-split interstitial. (Color online.)

Table 5. Arsenic interstitial structure energies (in eV), relative to ground state structure. A vb denotes that the defect levels are below the VB edge. If the structure is unstable and relaxes to a different structure, that structure name is listed in the table instead of the energy.

Charge	Func.	$T_{i,a}$ T_d	$T_{i,g}$ T_d	H C_{3v}	$1\,1\,0_a$ C_{2v}	$0\,0\,1_g$ C_{2v}	p-$0\,0\,1_g$ C_{1h}	$1\,1\,0_g$ C_{1h}	B_g C_{1h}
	LDA	—	—	—	**0**	0.71	$0\,0\,1_g$	0.92	0.56
$As_i(1-)$	LDA-3d	—	—	—	**0**	0.72	$0\,0\,1_g$	0.87	0.51
	PBE	—	—	—	**0**	0.46	$0\,0\,1_g$	0.77	0.38
	LDA	—	—	0.77	**0**	0.63	0.40	0.62	0.23
$As_i(0)$	LDA-3d	—	—	0.66	**0**	0.69	0.34	0.73	0.27
	PBE	—	—	0.67	**0**	0.59	0.23	0.71	0.19
	LDA	1.56	1.19	0.35	0.39	0.96	**0**	0.65	0.37
$As_i(1+)$	LDA-3d	1.43	1.10	0.29	0.29	0.98	**0**	0.58	0.41
	PBE	1.56	1.24	0.43	0.42	1.01	**0**	0.73	0.41
	LDA	0.41	0.18	0.01	vb	vb	vb	B_g	**0**
$As_i(2+)$	LDA-3d	0.36	0.20	**0**	vb	vb	vb	B_g	0.08
	PBE	0.36	0.24	0.02	vb	vb	vb	B_g	**0**
	LDA	0.10	**0**	0.44 ∼ vb	—	—	—	—	$T_{i.a}$
$As_i(3+)$	LDA-3d	0.02	**0**	0.26 ∼ vb	—	—	—	—	$T_{i.a}$
	PBE	**0**	0.04	0.39 ∼ vb	—	—	—	—	$T_{i.a}$

and 0.4 eV higher the the H site, for the $T_{i,g}$ and $T_{i,a}$ sites, respectively. The $As_i(2+)$ now distinctly prefers the $T_{i,g}$ site over the $T_{i,a}$ site, a preference that is magnified as the interstitial gains more electrons. An in-network B_g structure, depicted in figure 8, is already as stable as the non-bonded H site, within 0.1 eV, for $As_i(2+)$. Other in-network structures attempted for $As_i(2+)$ either relaxed into one of these structures or were embedded deep in the valence band

and were not valid defect states. This distortion from T_d for $As_i(2+)$ indicates that this is a true local defect state, in contrast to the result in $Ga_i(0)$ where the failure of the T_i structure to distort indicated that the defect was not a local defect state, but rather was involved in the CB.

The $As_i(1+)$ has the most varied landscape among all the charge states. The As-puckered $0\,0\,1_g$ split interstitial structure, p-$0\,0\,1_g$, yields the lowest energy. We find that this structure, first identified by Chadi [82], keeps a mirror plane C_{1h} symmetry. The As shares a lattice Ga site, oriented in the [0 0 1]-direction, both the As and Ga have three bonds, one to each other and two to neighboring As atoms on opposite sides of the site. In the ideal C_{2v}-$0\,0\,1_g$-split site, both As and Ga are planar. However, the number of electrons is perfect for As to pucker out of the plane of its three bonds to form a pyramid structure with a full lone pair, leaving the trivalent Ga atom in a planar configuration. This structure incorporates two of the structural motifs identified in the vacancy defects earlier. The B_g-site, the C_{2v}-$1\,1\,0_a$ split interstitial and also the non-bonded H site are within 0.3–0.4 eV of the p-$0\,0\,1_g$ ground state. The relative energies are remarkably insensitive to the functional or PP used in the calculations.

In $As_i(0)$, the C_{2v}-$1\,1\,0_a$-split interstitial becomes the ground state, and it remains the ground state for the $As_i(1-)$. The computed formation energy is insensitive to functional or PP, 3.58 eV in LDA, 3.46 eV in PBE and in LDA-3d. The B_g and p-$0\,0\,1_g$ structures remain competitive in the neutral charge state, within 0.2–0.4 eVy of the $1\,1\,0_a$ structure. In $As_i(1-)$, the p-$0\,0\,1_g$ unpuckers, regaining the C_{2v} symmetry of the ideal $0\,0\,1_g$-split configuration, and it, and the B_g, both become less stable relative to the $1\,1\,0_a$ ground state configuration.

With large lattice relaxations associated with significant structural changes as the charge state changes, the As_i has two negative-U systems. The $(1-/1+)$ transition slightly above midgap is due to the lattice relaxation from the $1\,1\,0_a$ structure to the p-$0\,0\,1_g$ structure in the positive charge state. We find the $(1-/1+)$ is a relatively weak negative-U, and disappears using the LDA-3d. A negative-U $(1-/1+)$ transition around this structural transition had been anticipated by Chadi [82], but using very small 32-site supercells and skimpy basis sets. Other, more recent work did not widely explore structural alternatives in As_i, one study predicting distinct positive-U $(1-/0)$ and $(0/1+)$ transitions for a $1\,1\,0_a$ structure [47], and a second study predicting the $1\,1\,0_a$ structure would be negative-U spanning the full four-electron $(1-/3+)$ transition [83].

We find a second, much stronger, negative-U transition for $(1+/3+)$. The lattice relaxation associated with global bistability between the non-network and in-network configurations is more significant. Also, the p-$0\,0\,1_g$ structure for $As_i(1+)$, expressing two favored chemical motifs, is unusually stable. Consequently, the $As_i(2+)$ proves not thermodynamically stable, the nominal $(1+/2+)$ transition is well below the VB edge. The removal of a second electron to form either $T_i(3+)$ defects stabilizes the defect sufficiently to bring the $(3+/1+)$ transition above the band edge by 0.06–0.08 eV.

Of all the simple defects, the calculations predict the arsenic interstitial to be the most mobile. Simple migration of either the $As_i(3+)$, or the $As_i(2+)$ through a non-bonded T–H–T path incurs a 0.4 eV barrier, with the H being a barrier in the $As_i(3+)$ and the minimum in $As_i(2+)$. The calculations for $As_i(1+)$ also suggest a rather flat potential energy surface, with a 0.4 eV deep well for the p-$0\,0\,1_g$ structure, and we anticipate low barriers for thermal diffusion for $As_i(1+)$, too. In p-type and semi-insulating GaAs, As_i should be more mobile than any of the other simple intrinsic defects in GaAs. The ∼0.4 eV barriers for As_i diffusion computed above would be in remarkably good agreement with the 0.5 eV determined as an As_i migration energy by Bourgoin *et al* [3].

Table 6. Formation energies of simple defects, in eV, in the As-rich limit, for each simulation context. Note that the $Ga_i(0)$ is thermodynamically unstable.

State	As_{Ga}	Ga_{As}	*aa*	v_{Ga}	v_{As}	*vv*	Ga_i	As_i
				LDA-3d				
n-type	1.48	1.10	2.26	−0.11	1.57	2.08	3.86	2.88
Neutral	1.48	2.80	2.26	2.50	3.41	4.05	(4.10)	3.51
p-type	0.24	2.03	2.26	1.90	2.54	3.55	2.14	2.44
				LDA				
n-type	1.50	1.45	2.52	0.01	1.88	2.31	4.07	2.88
Neutral	1.50	3.19	2.52	2.69	3.55	4.19	(4.53)	3.58
p-type	0.29	2.53	2.52	2.02	2.57	3.76	2.23	2.54
				PBE				
n-type	1.27	1.50	2.44	−0.02	1.80	2.16	3.90	2.85
Neutral	1.27	3.20	2.44	2.65	3.44	3.59	(4.20)	3.46
p-type	0.04	2.47	2.44	1.31	2.38	3.11	2.07	2.24

3.9. Formation energies

In table 6 we present the formation energies of the simple defects investigated in this study. We present the formation energy of each neutral defect, along with the formation energy of each defect with the Fermi levels at the CB edge and the VB edge, i.e. in the charge state and chemical potential appropriate to n-type and p-type GaAs, respectively. A neutral defect formation energy is, of course, insensitive to the Fermi level, hence the double antisite, with no levels in the gap, has a formation energy that is constant for the Fermi level across the gap. We note again that the $Ga_i(0)$ is not thermodynamically stable, hence the formation energy for the neutral is not physically meaningful. The charge states used are those presented in the level diagrams in figures 1 and 2. The values are presented in the arsenic-rich limit, as device materials are most commonly grown As-rich. However, these values can be straightforwardly translated into a gallium-rich limit knowing the stoichiometry of the defect and the computed heat of formation for GaAs [42].

The LDA, LDA-3d and PBE formation energies are broadly similar to each other. Differences in formation are larger than the differences in defect levels. Total formation energies are less accurately computed than relative energies in DFT, a cancellation of errors aids the accuracy of the relative defect levels. In As-rich material, the As_i and v_{Ga} will be the dominant defects for p-type and n-type material, respectively, with near-zero, and in the case of v_{Ga}, even slightly negative formation energies, a qualitative conclusion very similar to the very early DFT studies [77]. In as-grown material, the EL2, identified as the As_{Ga}, is observed to be the dominant defect. The v_{Ga} has remained invisible.

4. Analysis and discussion

The comprehensive agreement of the calculated properties of the As_{Ga} with the observed properties of the EL2—defect level positions and splitting, metastable structure and barriers—confirms that the DFT calculations are giving good predictions of GaAs defects. With a full survey of the intrinsic defects and their structure, charge states and energy levels, we can begin to assess their relationship to defect levels that are seen in experiment, and expand the understanding of defect behavior in GaAs.

Some consensus has developed that v_{As} is responsible for the E1 and E2 defect levels introduced in electron-irradiated GaAs [3]. The E1 level that appears at 32–45 meV below the

CB and the E2 level at 0.13–0.18 eV [5, 79, 88, 89] are known to be two distinct transitions of the same defect [5]. These were initially attributed to the $(2-/1)$ and $(1-/0)$ acceptor states v_{As} [79, 88], but analysis of a positron experiment concluded that the E1 and E2 transitions within a v_{As} model had to be $(1-/0)$ and $(0/1+)$, to explain the progression of positron trapping coefficients as the defect was progressively ionized [90]. Our calculations clearly contradict the identification of the E1 and E2 defect levels with v_{As}. First, $v_{\mathrm{As}}(1-/1+)$ is a midgap negative-U system, far from the CB edge. Second, v_{As} takes charge states up to $(3-)$. Setting aside the positron experiment analysis, and accepting the initial experiments suggesting that both E1 and E2 were acceptor states [88], emission from $v_{\mathrm{As}}(3-)$ could presumably lead to E1 and E2. However, our calculations show $v_{\mathrm{As}}(3-/1-)$ is a negative-U system, hence would have only one, not two levels, and that this transition is still too deep to be either the E1 and E2. We conclude the E1 and E2 levels cannot be attributed to v_{As}.

Having prompted a step backward, perhaps, in our understanding of GaAs defects, rejecting v_{As} as the defect responsible for the E1 and E2 levels, the DFT results offer a step forward again. The large number defects with defect levels at midgap and in the lower half of the band gap will make it difficult to make credible assignments of a defect structure to those levels. However, there are relatively few energy levels above midgap among the intrinsic defects. In particular, the divacancy has two levels very near the CB edge. The relatively shallow $(4-/3-)$ and $(3-/2-)$ levels are nearly degenerate in LDA (within 0.02 eV), and the puckering of the unpaired Ga atom in going beyond the $(2-)$ charge state causes a small negative-U ordering for $vv(4-/2-)$ in PBE. However, these calculations lack spin polarization. Spin polarization is not a large effect in any GaAs, but large enough to be important here. A spin-polarized calculation lowers the $vv(3-)$ energy by 0.03 eV (LDA) or 0.05 eV (PBE), resulting in a standard positive ordering, the $(4-/3-)$ level 0.08(0.05) eV above the $(3-/2-)$ level in LDA(PBE). The resulting $vv(4-/3-)$ and $vv(3-/2-)$ defect levels match the E1 and E2 levels observed in irradiated GaAs almost exactly. Experiments report E1 and E2 at $E_{\mathrm{c}}-0.032$ and $E_{\mathrm{c}}-0.129$ eV [89] or $E_{\mathrm{c}}-0.045$ and $E_{\mathrm{c}}-0.140$ eV [5], separated by 0.10 eV. There are no other intrinsic defects with levels near the CB. The DFT calculations clearly implicate the divacancy as responsible for the E1 and E2 levels in irradiated GaAs. To confirm this assignment, a few inconvenient, seemingly inconsistent, experimental observations would need to be explained; this will be presented elsewhere [91].

No longer conscripted to serve as the source of the E1 and E2, the v_{As} is now free to be assigned elsewhere. We propose that the E3 center in irradiated silicon [5], determined to be identical to the EL6 center seen in semi-insulating, as-grown GaAs, [56] is the v_{As}. The E3/EL6 energy level is reported to be 0.27–0.38 eV below the CB edge [5, 52, 54–56, 58, 92]. The only viable candidate in the computed survey of intrinsic defect levels is the negative-U $v_{\mathrm{As}}(3-/1-)$ transition, at -0.36 eV in LDA, -0.43 eV in PBE, in nearly perfect agreement with the E3 center level. No other intrinsic defects have levels this high in the band gap. The DX-like properties of the EL6 center [58] can be explained by the global bistability in v_{As}, as it shifts between the simple v'_{As} vacancy and the v^{*}_{As} ($\mathrm{Ga_{As}}$–v_{Ga} nearest neighbor pair) [91].

The identification of the E3 center with the v_{As} justifies treating the $\mathrm{Ga_{As}}$–v_{Ga} pair as a distorted manifestation of the simple As vacancy, and including it in computing levels for v_{As} as the v^{*}_{As}, as we have done here. The v_{Ga} level calculations also treated the simple and site-shifted form as a single defect system. In both cases, the site shift occurs across a change from positive to negative defect, driven by the strong electron affinity of As lone pairs and strong hole affinity to form trivalent Ga. These unified descriptions could be crucial to understand Fermi-level pinning in GaAs, the site-shifting, charge-switching vacancies are the basis of an amphoteric native defect model for understanding many phenomena in GaAs [93, 94].

The vacancies will not be highly mobile, based on a simple qualitative analysis. A sequence of nearest neighbor hops, with relatively modest barrier, moves the location of a vacant site, but leaves behind a trail of high-energy antisites. Transport of a simple monovacancy entails second-nearest neighbor hopping, or a concerted diffusion mechanism, requiring multiple bond-breaking events that will require significant energy. Computational studies for Ga vacancy diffusion [95] and As vacancy diffusion [96] confirm this qualitative description. No low-energy path was found, the migration barrier was reported to be more than 2 eV for both v_{Ga} and v_{As}. The current results, with a more comprehensive description of the static vacancies, more stable charge states incorporating the site-shifted forms, do not suggest any new migration pathways that might have lower migration barriers.

The current results do speak to the mobility of $\mathrm{Ga_i}$. The $\mathrm{Ga_i}$ will diffuse in its positive charge states, with a migration barrier of $\gtrsim$1 eV. The diffusion will be most favorable as $\mathrm{Ga_i}(+)$. These results contradict those from an earlier study [87]. The $\mathrm{Ga_i}$ calculations point out an important pitfall in simulations of diffusion barriers. If the output of the calculations were accepted without careful inspection, the $\mathrm{Ga_i}(0)$ would diffuse with a 0.6 eV barrier, from a minimum in a tetrahedral interstitial ground state site through a C_{2v}-1 1 0_{g}-split interstitial site (figure 8(*c*)). However, despite having the lowest energy of any $\mathrm{Ga_{As}}$ supercell calculation, the DFT 'ground states', the tetrahedral sites are *not* true defect states, and not legitimate pathways. To establish valid ground state defect structures and migration barriers, every configuration along a migration path must be verified to be a true defect state and not a computational artifact. This will make computation of barriers in the interstitials particularly challenging, as we encountered numerous configurations that had to be discarded because the KS eigenvalue of the defect was deeply embedded into a band.

The calculations confirm the general consensus that the As interstitial is the mobile species in GaAs. The simulations indicate barriers of $\gtrsim$0.4 eV, consistent with the 0.5 eV migration energy deduced from experiment [3]. While these calculations predict that the $\mathrm{As_i}$ will be a facile thermal diffuser, the results further predict that $\mathrm{As_i}$ will also likely diffuse through an athermal process [97, 98]. Taking advantage of the multistability with charge state, diffusion of $\mathrm{As_i}$ can be driven by the sequential capture of electron and holes. One obvious candidate for an athermal diffusion path is through $\mathrm{As_i}(2+/3+)$ non-bonded sites. A tetrahedral $\mathrm{As_i}(3+)$ in either T_{i} site captures an electron to become $\mathrm{As_i}(2+)$, the interstitial slides down the (2+) potential energy surface to the ground state H site in $\mathrm{As_i}(2+)$, at which point the interstitial could capture a hole to convert back to $\mathrm{As_i}(3+)$, sliding back to a different T_{i} site. More involved candidate paths could delve deeper into the charge states of $\mathrm{As_i}$. For example, we find that non-bonded T_{i} sites in $\mathrm{As_i}(0)$ and $\mathrm{As_i}(1-)$ spontaneously insert into the lattice if offset from T_d symmetry, into bond-bridge configurations. The B sites ultimately collapse back into $T_{\mathrm{i,a}}$ sites as electrons are removed. These candidate athermal processes will be more active in p-type than n-type material, consistent with the observation that the mobility of $\mathrm{As_i}$ is higher in p-type GaAs than in n-type materials, which had prompted Stievenard *et al* to suggest the possibility of athermal migration mechanisms for $\mathrm{As_i}$ [99].

The arsenic interstitial and its levels are therefore unlikely to be observed by any electronic probe in GaAs. The gallium interstitial, with a high formation energy, will not be present in equilibrium GaAs, but could potentially exist in radiation-damaged GaAs. The signature would be two defect levels near the VB. The challenge would be distinguishing those levels from all the other intrinsic defects with levels near the VB, such as each of the vacancy defects. The arsenic antisite is the EL2, and we have proposed that the v_{As} and vv have both been observed in GaAs, once correct assignments are made. The big enduring mystery of GaAs is where is the v_{Ga}?

5. Summary and conclusions

We have presented a computational survey of defect structures and energy levels for simple intrinsic defects in GaAs, carefully testing the adequacy of various aspects of the computational models. The principal conclusions from the assessment of the computational models can be summarized as follows:

- The KS band gap problem is not a problem for GaAs defect calculations, the LDA, LDA-3D and PBE all give good defect band gaps despite significant (and different) KS band gap problems.
- A 3d-core PP for Ga is likely sufficient, differences from results with a 3d-valence PP are modest.
- The LDA and PBE give qualitatively the same results. The LDA yields better description of bulk properties [21], and LDA and PBE give mostly similar results for the defects, but PBE might be needed for better accuracy in describing stretched Ga–Ga bond pairs in vacancy defects.
- Spin polarization is not numerically significant, except for the divacancy, where the small effect of spin is enough to reveal the crucial character the divacancy plays in irradiated GaAs.
- Detailed control of boundary conditions is crucial to get good results, and FDSM [20] is quantitatively effective for extrapolating from the finite supercells to the bulk limit.
- The 216-site supercell calculations yield size-converged results for defect energy levels in GaAs, converged to less than the intrinsic accuracy of DFT. There is no need for 1000-site, or even 500-site, supercells, except for calibration and verification of the approximations in selected cases. The results extrapolated from 64-site supercell calculations are already numerically converged in many cases.
- The defect calculations must be carefully monitored for contamination with bulk band states. The lowest energy *supercell* calculation may not be the lowest energy *defect* structure. Migration barrier calculations may be particularly challenging.

With the close alignment of the 216-site and 512-site results across all the defect energy levels, the results are demonstrated to be converged with respect to the computational models. The detailed properties of the EL2 are reproduced by the simulations of the As_{Ga}. With this foundation, good confidence can be placed in the quantitative accuracy of the simulations of defect levels. Broad comparison with experiments in silicon showed an average error of 0.1 eV, and a maximum error of $\sim$0.2 eV, in predictions of defect energy levels. Underpinning this is the calculation of all defect levels for all defects with a single consistent method, with rigorous boundary conditions fixed, a single common electron reservoir for electron charge. None of the comparisons with the (sparse) experimental data in GaAs indicate the theory should perform any differently for the GaAs defects.

The comprehensive survey of simple intrinsic defects, without pre-judgement regarding their relevance or structure, provides a full catalogue of the primary defects that might be observed in GaAs. With this complete catalogue at hand, with all the defect levels consistently calculated, we can begin to correlate the intrinsic defects with phenomena observed in experiment. The principal findings in this work concerning the behavior of defects in GaAs are the following:

- Even the 'simple' intrinsic defects in GaAs are very complicated, with more charge states, bistabilities and negative-U transitions than anticipated.

- The monovacancies have a global bistability between simple vacancy and a vacancy–antisite pair, and this site-shift bistability must be included in a useful description of a monovacancy.
- Despite the unexpected complexity, simple chemical bonding motifs mostly account for all ground state structures.
- Interstitials will be responsible for observed defect evolution in radiation-damaged devices, with relatively low thermal barriers for diffusion.
- In addition, the arsenic interstitial will diffuse athermally.
- The neglected divacancy is an important player in radiation-damaged GaAs, it is responsible for the E1–E2 centers seen in electron-irradiated GaAs.
- The As vacancy is reassigned from the E1–E2 center to the E3 center.

The simple chemical picture that emerges, dominated by a few dominant structural motifs—three-fold pyramidal As with full lone pairs, three-fold trivalent Ga, stretched Ga–Ga cross-vacancy bonds—is not just an aesthetically pleasing conceptual framework, it is an immensely useful aid in searching for candidate low-energy structures in what are often very complicated potential energy surfaces for GaAs defects. The universality of these bonding motifs is demonstrated in studies of amorphous GaAs: Fois *et al* [100] identified the same three-fold As and Ga motifs as the dominant structures with levels near the band edges in a-GaAs, just as we find these dominate the electronic transitions in defects in crystalline GaAs.

The most obvious identifications, the vv and v_{As}, are a step forward, but there is still much unknown about intrinsic defects (e.g., the invisible v_{Ga}). And we did not begin to address defect complexes, which play significant roles in GaAs. The current results provide a baseline for understanding defects, and confidence that DFT results are quantitatively meaningful. We have demonstrated that first-principle theory finally is ready to meet the challenge laid down by Hurle [4], that it has achieved an accuracy in predicting defect properties sufficient to serve as a full partner to experiment, to begin to unravel the detailed, *quantitative* mysteries of defect physics in GaAs.

Acknowledgments

The authors are grateful to Robert Fleming and David Lang for helping them decipher the extensive experimental lore on radiation-damaged GaAs. They thank Harold P Hjalmarson and Arthur H. Edwards for useful discussions regarding the modeling of defects in semiconductors and GaAs. Calculations were performed on the Thunderbird Linux Cluster at Sandia, and the authors extend their gratitude for the Capacity Computing and Visualization Team for their support on the Tbird systems. The authors acknowledge the QASPR (Qualification Alternatives for the Sandia Pulsed Reactor) project for financial support of this work, and OAvL acknowledges support from the Sandia Truman Fellowship Program, LDRD Project No 120209. Sandia is a multiprogram laboratory operated by Sandia Corporation, a Lockheed Martin Company, for the United States Department of Energy's National Nuclear Security Administration under contract DE-AC04-94AL85000.

References

[1] Pilcher P 2004 *Intrinsic Point Defects, Impurities, and Their Diffusion in Silicon* (Wien: Springer)
[2] Lang D V 1977 Review of radiation-induced defects in III–V compounds *Inst. Phys. Conf. Ser.* **31** 70
[3] Bourgoin J C, Bardeleben H J and Stiévenard D 1988 Native defects in gallium arsenide *J. Appl. Phys.* **64** R65

[4] Hurle D T J 1999 A comprehensive thermodynamic analysis of native point defect and dopant solubilities in gallium arsenide *J. Appl. Phys.* **85** 6957
[5] Pons D and Bourgoin J C 1985 Irradiation-induced defects in GaAs *J. Phys. C: Solid State Phys.* **18** 3839
[6] Hohenberg P and Kohn W 1964 Inhomogeneous electron gas *Phys. Rev.* **136** B864
[7] Kohn W and Sham L J 1965 Self-consistent equations including exchange and correlation effects *Phys. Rev.* **140** A1133
[8] Baraff G A and Schlüter M 1985 Electronic structure, total energies, and abundances of elementary point defects in GaAs *Phys. Rev. Lett.* **55** 1327
[9] Zhang S B and Northrup J E 1991 Chemical potential dependence of defect formation energies in GaAs: application to Ga self-diffusion *Phys. Rev. Lett.* **67** 2339
[10] Sham L J and Schlüter M 1983 Density-functional theory of the energy gap *Phys. Rev. Lett.* **51** 1888
Sham L J and Schlüter M 1985 Density-functional theory of the band gap *Phys. Rev.* B **32** 3883
[11] El-Mellouhi F and Mousseau N 2005 Self-vacancies in gallium arsenide: an *ab initio* calculation *Phys. Rev.* B **71** 125207
[12] Messmer R P, McCarroll B and Singal C M 1972 Molecular orbital approach to chemisorption: IV. LCAO band structures and the molecular unit cell *J. Vac. Sci. Technol.* **9** 891
[13] Cohen M L, Schlüter M, Chelikowsky J R and Louie S G 1975 Self-consistent pseudopotential method for localized configurations: molecules *Phys. Rev.* B **12** 5575
[14] Makov G and Payne M C 1995 Periodic boundary conditions in *ab initio* calculations *Phys. Rev.* B **51** 4014
[15] Castleton C W M, Höglund A and Mirbt S 2006 Managing the supercell approximation for charged defects in semiconductors: finite-size scaling, charge correction factors, and band-gap problem, and the *ab initio* dielectric constant *Phys. Rev.* B **73** 035215
[16] Lany S and Zunger A 2008 Assessment of correction methods for the band-gap problem and for finite-size effects in supercell defect calculations: case studies for ZnO and GaAs *Phys. Rev.* B **78** 235104
[17] Freysoldt C, Neugebauer J and Van de Walle C G 2009 Fully *ab initio* finite-site corrections for charge-defect supercell calculations *Phys. Rev. Lett.* **102** 016402
[18] Schultz P A 1999 Periodic supercells and electrostatic boundary conditions *Phys. Rev.* B **60** 1551
[19] Schultz P A 2000 Charged local defects in extended systems *Phys. Rev. Lett.* **84** 1942
[20] Schultz P A 2006 Theory of defect levels and the 'band gap problem' in silicon *Phys. Rev. Lett.* **96** 246401
[21] von Lilienfeld O A and Schultz P A 2008 Structure and band gaps of Ga-(V) semiconductors: the challenge of Ga pseudopotentials *Phys. Rev.* B **77** 115202
[22] Mattsson A E, Schultz P A, Mattsson T R, Leung K and Desjarlais M P 2005 Designing meaningful density functional theory calculations in material science—a primer *Modelling Simul. Mater. Sci. Eng.* **13** R1
[23] Schultz P A *SEQQUEST code* (unpublished) see http:/dft.sandia.gov/Quest
[24] Perdew J P and Zunger A 1981 Self-interaction correction for density-functional approximations for many-electron systems *Phys. Rev.* B **23** 5048
[25] Perdew J P, Burke K and Ernzerhof M 1996 Generalized gradient approximation made simple *Phys. Rev. Lett.* **77** 3865
[26] Blakemore J S 1982 Semiconducting and other major properties of gallium arsenide *J. Appl. Phys.* **53** R123
[27] Vurgaftman I, Meyer J R and Ram-Mohan L R 2001 Band parameters for III–V compound semiconductors and their alloys *J. Appl. Phys.* **89** 5815
[28] Lide D R (ed) 1991 *Handbook of Chemistry and Physics* 72nd edc (Boca Raton: CRC Press)
[29] Sharma B D and Donohue J 1962 A refinement of the crystal structure of gallium *Z. Kristallogr.* **117** 293
[30] Beister H J, Strösser K and Syassen K 1990 Rhombohedral to simple-cubic phase transition in arsenic under pressure *Phys. Rev.* B **41** 5535
[31] Johnson D D 1988 Modified Broyden's method for accelerating convergence in self-consistent calculations *Phys. Rev.* B **38** 12807
[32] Jonsson H, Mills G and Jacobsen K W 1998 Nudged elastic band method for finding minimum energy paths of transitions *Classical and Quantum Dynamics in Condensed Phase Simulations* ed B J Berne *et al* (Singapore: World Scientific) p 385
[33] Jost W 1933 Diffusion and electrolytic conduction in crystals (ionic semiconductors) *J. Chem. Phys.* **1** 466
[34] Lento J, Mozos J-L and Nieminen R M 2002 Charged point defects in semiconductors and the supercell approximation *J. Phys. Condens. Matter* **14** 2637
[35] Sham L J and Kohn W 1966 One-particle properties of an inhomogeneous electron gas *Phys. Rev.* **145** 561
[36] Dabrowski J and Scheffler M 1988 Theoretical evidence for an optically inducible structural transition of the isolated As antisite in GaAs: identification and explanation for of EL2? *Phys. Rev. Lett.* **60** 2183
[37] Weber E R 1982 Identification of arsenic antisites in plastically deformed GaAs *J. Appl. Phys.* **53** 6140

[38] Lagowski J, Lin D G, Chen T-P, Skowronski M and Gates H C 1985 Native hole trap in bulk GaAs and its association with the double-charge state of the arsenic antisite defect *Appl. Phys. Lett.* **47** 929
[39] Omling P, Silverberg P and Samuelson L 1988 Identification of a second energy level of EL2 in n-type GaAs *Phys. Rev.* B **38** 3606
[40] Kamińska M, Skowroński M and Kushko W 1985 Identification of the 0.82-eV electron trap, EL2 in GaAs, as an isolated antisite arsenic defect *Phys. Rev. Lett.* **55** 2204
[41] Nissen M K, Villemaire A and Thewalt M L W 1991 Photoluminescence studies of the EL2 defect in gallium arsenide under external perturbation *Phys. Rev. Lett.* **67** 112
[42] Zhang Q-M and Bernholc J 1993 As_{Ga}–X_I complexes as models for the EL2 center in GaAs *Phys. Rev.* B **47** 1667
[43] Morrow R A 2002 Defect formation in GaAs grown by organometallic vapor phase epitaxy and the structure of the native defect EL2 *J. Cryst. Growth* **241** 57
[44] Chadi D J and Chang K J 1988 Metastabiliy of the isolated arsenic-antisite defect in GaAs *Phys. Rev. Lett.* **60** 2187
[45] Northrup J E and Zhang S B 1993 Dopant and defect energetics: Si in GaAs *Phys. Rev.* B **47** 6791
[46] Zollo G, Tarus J and Nieminen R M 2004 Reliability of analytical potentials for point defect simulations in GaAs *J. Phys. Condens. Matter* **16** 3923
[47] Schick J T, Morgan C G and Papoulias P 2002 First-principles study of As interstitials in GaAs: convergence, relaxation and formation energy *Phys. Rev.* B **66** 195302
[48] Vincent G, Bois D and Chantre A 1982 Photoelectric memory effect in GaAs *J. Appl. Phys.* **53** 3643
[49] Kuisma S, Saarinen K, Hautojärvi P and Corbel C 1997 Microscopic nature and optical properties of metastable defects in electron-irradiated GaAs *Phys. Rev.* B **55** 9609
[50] Fukuyama A, Ikari T, Akashi Y and Suemitsu M 2003 Interdefect correlation during thermal recovery of the *EL2* in semi-insulating GaAs: Proposal of a three-center complex model *Phys. Rev.* B **67** 113202
[51] Bencherifa A, Brémond G, Nouailhat A, Guilot G, Guivarc'h A and Regreny A 1987 On the identification of the double donor state of EL2 in p type GaAs *Rev. Phys. Appl.* **22** 891
[52] Chantre A, Vincent G and Bois D 1981 Deep-level optical spectroscopy in GaAs *Phys. Rev.* B **23** 5335
[53] Samuelson L, Omling P, Pitze H and Grimeis H G 1981 Electrical and optical properties of deep levels in MOVPE grown GaAs *J. Cryst. Growth* **55** 164
[54] Fang Z Q, Schlesinger T E and Milnes A G 1987 Evidence for EL6 ($E_c - 0.35$ eV) acting as the dominant recombination center in n-type horizontal Bridgman GaAs *J. Appl. Phys.* **61** 5047
[55] Min S K, Kim E K and Cho H Y 1988 Abnormal behavior of midgap electron traps in HB-GaAs during thermal annealing *J. Appl. Phys.* **63** 4422
[56] Hashizume T and Nagabuchi H 1989 Characterization of deep electron states in LEC grown GaAs materials *Semicond. Sci. Technol.* **4** 427
[57] Jorio A, Wang A, Parenteau M, Carlone C, Rowell N L and Khanna S M 1994 Optical identification of the gallium vacancy in neutron-irradiated gallium arsenide *Phys. Rev.* B **50** 1557
[58] Reddy C V, Luo Y L, Fung S and Beling C D 1998 DX-like properties of the EL6 defect family in GaAs *Phys. Rev.* B **58** 1358
[59] Chadi D J 2003 Arsenic antisite defect in GaAs: multiplicity of charge and spin states *Phys. Rev.* B **68** 193204
[60] Gorczyca I, Christensen N E and Svane A 2002 Influence of hydrostatic pressure on cation vacancies in GaN, AlN, and GaAs *Phys. Rev.* B **66** 075210
[61] Yu P W, Mitchell W C, Mier M G, Li S S and Wang W L 1982 Evidence of intrinsic double acceptor in GaAs *Appl. Phys. Lett.* **41** 532
[62] Elliott K R 1983 Residual double acceptors in bulk GaAs *Appl. Phys. Lett.* **42** 274
[63] Yu P W, Fischer D W and Sizelove J R 1992 Photoluminescence of Ga_{As}-related 1.32 emission in bulk GaAs *Semicond. Sci. Technol.* **7** 556
[64] Zhang S B and Chadi D J 1990 Cation antisite defects and antisite-interstitial complexes in GaAs *Phys. Rev. Lett.* **64** 1789
[65] Seong H and Lewis L J 1995 Tight-binding molecular dynamics of point defects in GaAs *Phys. Rev.* B **52** 5675
[66] Jahn H and Teller E 1937 Stability of polyatomic molecules in degenerate electronic states: I. Orbital degeneracy *Proc. R. Soc. Lond. Ser. A* **161** 220
[67] Cheong B-H and Chang K J 1994 Compensation and diffusion mechanisms of carbon dopants in GaAs *Phys. Rev.* B **49** 17436
[68] Pöykkö S, Puska M J and Nieminen R M 1997 Metastability of the antistructure pair in GaAs *Phys. Rev.* B **55** 6914
[69] Baraff G A and Schlüter M 1985 Bistability and metastability of the gallium vacancy in GaAs: the actuator of *EL2*? *Phys. Rev. Lett.* **55** 2340

[70] Pöykkö S, Puska M J, Alatalo M and Nieminen R M 1996 Metastable defect complexes in GaAs *Phys. Rev.* B **54** 7909
[71] Janotti A, Wei S-H, Zhang S B, Kurtz S and Van de Walle C G 2003 Interactions between nitrogen, hydrogen, and gallium vacancies in $GaAs_{1-x}N_x$ alloys *Phys. Rev.* B **67** 161201
[72] Baraff G A and Schlüter M 1986 Binding and formation energies of native defect pairs in GaAs *Phys. Rev.* B **33** 7346
[73] Laasonen K, Nieminen R M and Puska M J 1992 First-principle study of fully relaxed vacancies in GaAs *Phys. Rev.* B **45** 4122
[74] Gilgien L, Galli G, Gygi F and Car R 1994 *Ab initio* study of positron trapping at a vacancy in GaAs *Phys. Rev. Lett.* **72** 3214
[75] Puska M J 1989 Electronic structure of point defects in III–V compound semiconductors *J. Phys. Condens. Matter* **1** 7347
[76] Pöykko S, Puska M J and Nieminen R M 1996 *Ab initio* study of fully relaxed divacancies in GaAs *Phys. Rev.* B **53** 3813
[77] Northrup J E and Zhang S B 1994 Energetics of the As vacancy in GaAs: the stability of the 3+ charge state *Phys. Rev.* B **50** 4962
[78] Puska M J and Corbel C 1988 Positron states in Si and GaAs *Phys. Rev.* B **38** 9874
[79] Corbel C, Stucky M, Hautojärvi P, Saarinen K and Moser P 1988 Positron-annihilation spectroscopy of native vacancies in as-grown GaAs *Phys. Rev.* B **38** 8192
[80] Bösker G, Stolwijk N A and Hettwer H-G 1995 Use of zinc diffusion into GaAs for determining properties of gallium arsenide *Phys. Rev.* B **52** 11927
[81] Bracht H and Brotzmann S 2005 Zinc diffusion in gallium arsenide and the properties of gallium interstitials *Phys. Rev.* B **71** 115216
[82] Chadi D J 1992 Self-interstitial bonding configurations in GaAs and Si *Phys. Rev.* B **46** 9400
[83] Zollo G and Nieminen R M 2003 Small self-interstitial clusters in GaAs *J. Phys.: Condens. Matter* **15** 843
[84] Zollo G, Lee Y J and Nieminen R M 2004 Properties of intrinsic di-interstitials in GaAs *J. Phys.: Condens. Matter* **16** 8991
[85] Volpe M, Zollo G and Colombo L 2005 Structural, electronic, and energetic properties of small interstitial clusters in GaAs by tight-binding molecular dynamics *Phys. Rev.* B **71** 075207
[86] Malouin M-A, El-Mellouhi F and Mousseau N 2007 Gallium self-interstitial relaxation in GaAs: an *ab initio* characterization *Phys. Rev.* B **76** 045211
[87] Levasseur-Smith K and Mousseau N 2008 Numerical characterization of the Ga interstitial self-diffusion mechanisms in GaAs *J. Appl. Phys.* **103** 113502
[88] Loualiche S, Nouailhat A, Guillot G and Lannoo M 1984 Interpretation of deep-level optical spectroscopy and deep-level transient spectroscopy data: application to irradiation defects in GaAs *Phys. Rev.* B **30** 5822
[89] Lai S T and Nener B D 1994 Annealing behavior of deep-level defects in 1 MeV electron-irradiated GaAs *J. Appl. Phys.* **75** 2354
[90] Saarinen K, Hautojärvi P, Lanki P and Corbel C 1991 Ionization levels of As vacancies in as-grown GaAs studied by positron-lifetime spectroscopy *Phys. Rev.* B **44** 10585
[91] Schultz P A 2009 unpublished
[92] Martin G M, Estéve E, Langlade P and Makram-Ebeid S 1984 Kinetics of formation of the midgap donor EL2 in neutron irradiated GaAs materials *J. Appl. Phys.* **56** 2655
[93] Walukowski W 1989 Amphoteric native defects in semiconductors *Appl. Phys. Lett.* **54** 2094
[94] Ky N H and Reinhart F K 1998 Amphoteric native defect reactions in Si-doped GaAs *J. Appl. Phys.* **83** 718
[95] El-Mallouhi F and Mousseau N 2006 Charge-dependent migration pathways for the Ga vacancy in GaAs *Phys. Rev.* B **74** 205207
[96] El-Mallouhi F and Mousseau N 2007 *Ab initio* characterization of arsenic diffusion pathways in GaAs with SIEST-A-RT *Appl. Phys.* A **86** 309
[97] Watkins G D 1965 A review of EPR studies in irradiated silicon *Radiation Damage in Semiconductors* ed P Baruch (Paris: Dunod) p 97
[98] Bourgoin J C and Corbett J W 1972 A new mechanism for interstitial migration *Phys. Lett.* A **38** 135
[99] Stievenard D, Boddaert X, Bourgoin J C and Bardeleben H J 1990 Behavior of electron-irradiation-induced defects in GaAs *Phys. Rev.* B **41** 5271
[100] Fois E, Selloni A, Pastore G, Zhang Q-M and Car R 1992 Structure, electronic properties, and defects of amorphous gallium arsenide *Phys. Rev.* B **45** 13378